

ENHANCED THERMOPHOTOVOLTAIC SYSTEMS USING ONE  
DIMENSIONAL PHOTONIC CRYSTAL OPTICAL FILTERS WITH A  
GRADED INDEX OF REFRACTION PROFILE

MEHRAN SEPAH MANSOOR

A THESIS SUBMITTED TO  
THE FACULTY OF GRADUATE STUDIES  
IN PARTIAL FULFILLMENT OF THE REQUIREMENTS  
FOR THE DEGREE OF  
MASTER OF APPLIED SCIENCE

GRADUATE PROGRAM IN MECHANICAL ENGINEERING

YORK UNIVERSITY

TORONTO, ONTARIO

DEC 2023

© Mehran Sepah Mansoor, 2023

## Abstract

This thesis investigates the enhancement of thermophotovoltaic (TPV) systems using one-dimensional photonic crystals (1DPC) with a graded index of refraction as optical filters. It compares three 1DPC configurations: graded index, traditional quarter-wave, and modified quarter-wave stacks, to improve TPV performance. Designed for TPV applications, these filters aim to increase in-band transparency and minimize absorption while ensuring high out-of-band reflection. Graded index 1DPCs, made of porous silicon dioxide and solid zirconium dioxide, exhibit low absorbance across a broad spectrum, offering a novel approach in TPV applications.

Significantly, a double-stack graded filter at an emitter temperature of 2000 K achieved 74% in-band transmittance and 55% out-of-band reflectance. Highlighting a design trade-off, the study presents an optimal filter configuration that yields a 24% system efficiency and a power density of  $6.9 \text{ W/cm}^2$ . The analysis focuses on system efficiency and power output, emphasizing the advancement in TPV efficiency through the application of graded index 1DPC filters.

## Acknowledgement

I express my profound gratitude to Professor Paul G. O'Brien, my research advisor, for his invaluable guidance, enduring patience, and profound expertise throughout the course of my graduate studies and research. His astute mentorship and unwavering support were instrumental during every phase of my research and writing of this thesis.

I also would like to extend my sincere appreciation to Professor Nima Tabatabaei, a valued member of my committee, for his invaluable insights, constructive feedback, and thought-provoking questions. His contributions have significantly enriched the depth and quality of this work. I am also deeply indebted to Dr. Nima Talebzadeh for their insightful feedback and pivotal suggestions, which significantly augmented the caliber of this work.

I must express heartfelt thanks to my parents, friends, and other members of AMSET lab research group. Their constant support and relentless encouragement were foundational throughout my academic journey and the meticulous process of thesis development.

This work was carried out during my tenure at the Mechanical Engineering Department of York University. My gratitude extends to the Bergeron Centre for Engineering Excellence and the Lassonde School of Engineering, both of which offered exceptional research environments and substantial financial assistance.

Toronto, Oct 10th, 2023

Mehran Sepah Mansoor

# Table of Contents

Abstract .....	II
Acknowledgement .....	iii
Table of Contents .....	iv
List of Figures .....	vii
List of Tables .....	x
List of Symbols .....	xi
List of Acronyms .....	xiii
1 Introduction .....	1
1.1 Global Warming .....	2
1.2 Energy Production Globally and In Canada .....	2
1.3 Renewable Energy Resources .....	4
1.4 History of Thermophotovoltaic .....	5
1.5 Applications of Thermophotovoltaic .....	6
1.5.1 Thermal Energy Grid Storage .....	7
1.6 Research Gaps .....	9

1.7	Objective .....	10
1.8	Overview .....	11
2	Background .....	14
2.1	Thermophotovoltaic Systems .....	14
2.1.1	Emitters in Thermophotovoltaic .....	16
2.1.2	PV Cells in Thermophotovoltaic Systems .....	17
2.1.3	Spectral Control in Thermophotovoltaic Systems .....	19
2.1.4	Front Cold Side Filters .....	20
2.2	Photonic Crystal .....	21
2.2.1	One-Dimensional Photonic Crystals .....	24
2.2.2	Two-Dimensional Photonic Crystals .....	26
2.2.3	Three-Dimensional Photonic Crystals .....	27
2.3	Optical Properties Of Nanoparticles .....	27
2.3.1	Preparation of Nanoparticle Films For Optical Application .....	28
2.3.2	Coating Techniques For Making Nanoparticle Films .....	29
2.4	Fabrication And Characterization Of Graded Index One-Dimensional Photonic Crystal Thin Films .....	29

2.5	Energy Balance In Thermophotovoltaic Components .....	31
3	Methodology .....	35
3.1	Description Of Thermophotovoltaic System And One-Dimensional Photonic Crystal Optical Filters .....	35
3.2	Methods For Determining Filter Reflectance, Transmittance, And Absorptance .....	41
3.3	Calculating TPV System Efficiency and Electrical Power Output .....	45
3.4	Wave Optics Module In Comsol Multiphysics .....	50
4	Results .....	54
4.1	Optical Evaluation of Designed Filters .....	54
4.2	Evaluation of TPV System with the Designed Optical Filters .....	61
5	Discussion .....	65
6	Conclusion .....	72
7	References .....	74

## List of Figures

Figure 1. TPV energy conversion	1
Figure 2. Global primary energy consumption from different resources [2]	3
Figure 3. Canada energy consumption by source [2]	4
Figure 4. Antora Energy's battery running at a facility in Fresno, California [18]	6
Figure 5. The concept of thermal energy grid storage system using TPV [28]	8
Figure 6. TPVs system: (a) Energy conversion in TPVs, (b) Schematic of a TPV system with an optical filter placed on top of the PV cell, (c) Concept of radiation spectrum, bandgap, and BB radiation in TPVs.	15
Figure 7. Schematic of PV cell for TPV application equipped with an optical filter.	18
Figure 8. Structural variations of PCs: (a) 1D, (b) 2D, and (c) 3D configuration.	22
Figure 9. Photonic band diagram for a) 1DPC, b) 2DPC and c) 3DPC	23
Figure 10. SEM images of a TiO <sub>2</sub> /SiO <sub>2</sub> 1DPC with graded index of refraction [114]	31
Figure 11. Total reflectance at $\lambda=633$ nm, 830 nm, and 904 nm for both quarter-wave and graded-index AR-coating samples [114].	31
Figure 12. BB radiation spectra at different temperatures.	33

Figure 13. Spectral control in a TPV system with a front side optical filter. (b) Schematic diagram of a 1D PC in the form of a quarter-wave stack, a 1DPC filter with graded indices of refraction at its internal interfaces and a quarter-wave stack wherein the thickness of its top layer is reduced to half the thickness of the other layers within the stack.	36
Figure 14. Normal reflectance for 1DPC with $H[LH]^2$ , $H[LH]^3$ , $H[LH]^4$ and $H[LH]^5$ .	38
Figure 15. (a) Refractive index ( $n$ ) and extinction coefficient ( $\kappa$ ) spectra of $ZrO_2$ and 30% porous $SiO_2$ . (b) Refractive index profile for quarter-wave stack and graded index filters.	40
Figure 16. Graded index(quintic) and quarter wave stack profiles.	43
Figure 17. (a) TM and (b) TE polarization of 1D $ZrO_2/SiO_2$ PC in form of $[L/2H][LH]^4[LH]^5$ at different incident angles.	44
Figure 18. Reflectance of $L/2H[LH]^4$ with different index of refraction for glass substrate.	45
Figure 19. Quarter-wave and graded index 1DPC simulation in COMSOL interface.	53
Figure 20. Normal-angle spectral (a) reflectance and (b) transmittance of the designed one stack 1DPC filters in three arrangements of $H[LH]^5$ , $[L_Q/2 H_Q L_Q/2]^5$ and $[L/2 H][LH]^4$ . Normal-angle (c) reflectance and (d) transmittance of the designed double stack 1DPC filters in three arrangements of $H[LH]_{2.4} [LH]_{3.4}$ , $[L_Q/2 H_Q L_Q/2]_{2.2} [L_Q/2 H_Q L_Q/2]_{3.6}$ and $[L/2 H][LH]_{2.4} [LH]_{3.4}$ index.	56
Figure 21. Optical behavior of six designed filters in terms of transmittance, reflectance, and absorptance for (a) in-band region and (b) out-of-band region at different emitter temperatures.	60

Figure 22. Optimizing spectral efficiency (a), (b) and TPV system efficiency (c), (d) and power output (f) at 1800K emitter temperature with varying peak positions in the following cases: (1)  $H[LH]^5$ , (2)  $[LQ/2 H_Q LQ/2]^5$ , (3)  $[L/2H][LH]^4$ , (4)  $H[LH]^5[LH]^5$ , (5)  $[LQ/2H_Q LQ/2]^5 [LQ/2H_Q LQ/2]^5$  and (6)  $[L/2H][LH]^4[LH]^5$ . 63

Figure 23. (a) Spectral efficiency and (b) TPV system efficiency as a function of the in-band transmittance and out-of-band reflectance when the emitter is at a temperature of 1800 K and absorption in the filter is neglected. 68

## I. List of Tables

Table 1. Notation, structure, and peak position of the six TPV filters	36
Table 2. Peak position, low and high refractive index layer thickness.	41
Table 3. Comparison between six designs of 1DPC and case with no filter at 1800 K.	64
Table 4. Designed and fabricated optical filters in TPV.	70

## II. List of Symbols

Nomenclature	
Roman symbols	
$d_H$	thickness of layers with high refractive index
$d_L$	thickness of layers with low refractive index
$E_g$	energy bandgap of PV cells (eV)
$F_{\text{emit-PV}}$	view factor from emitter to PV cell
$F_{\text{PV-emitter}}$	view factor from PV cell to emitter
H	layers with high refractive index
$H_Q$	layers with quintic profile, high refractive index side
h	Planck's constant
$I_0$	spectral intensity
$\kappa$	extinction coefficient
$k_b$	Boltzmann's constant

L	layers with low refractive index
$L_Q$	layers with quintic profile, low refractive index side
n	real part of complex refractive index
$n_i$	incident media refractive index
$n_H$	refractive index of dense $ZrO_2$ ceramics
$n_L$	refractive index of 30% porous $SiO_2$ aerogels
$n_s$	refractive index of the substrate media
P	number of periods in filter designs
$P_{\text{PV}}$	power density output from the PV cell
$q_{\text{rad}}$	total emissive power
$P_{\text{input}}$	power supplied to the emitter to maintain its temperature
T	temperature of the blackbody (K)

$T_0$	temperature of the PV cell (K)
TE	transverse electric mode
TM	transverse magnetic mode
$\bar{T}$	average transmittance of TE and TM modes
$\bar{R}$	average reflectance of TE and TM modes
$\bar{A}$	average absorbance of TE and TM modes
$\bar{T}_{in-band}^P$	in-band transmitted power
$\bar{R}_{out-of-band}^P$	out-of-band reflected power
$\bar{A}_{total}^P$	total absorbed power
$\bar{T}_\lambda(\lambda, \theta)$	spectral directional transmittance
$\bar{R}_\lambda(\lambda, \theta)$	spectral directional reflectance
$\bar{A}_\lambda(\lambda, \theta)$	spectral directional absorbance
$\varepsilon$	emissivity
$\varepsilon_{\lambda, PV}$	emissivity of the PV cell when the wavelength is equal to $\lambda$

$\eta_{spec}$	spectral efficiency (%)
$\eta_{TPV}$	system efficiency (%)
$\theta$	angle of incidence (degree)
$\lambda_0$	central wavelength of the photonic bandgap ( $\mu\text{m}$ )
$\lambda_g$	cut-off bandgap of the PV cell ( $\mu\text{m}$ )
$\phi$	polar angle (steradian)
$\Omega$	solid angle
$\bar{T}_{out-of-band}^P$	out-of-band transmitted power
$\bar{R}_{in-band}^P$	in-band reflected power
$\bar{A}_{in-band}^P$	in-band absorbed power
$\bar{A}_{in-band}^P$	in-band absorbed power
$\bar{A}_{out-of-band}^P$	out-of-band absorbed power

### III. List of Acronyms

Nomenclature	
1D	One-Dimensional
1DPC	One-Dimensional Photonic Crystal
2D	Two-Dimensional
2DPCs	Two-Dimensional Photonic Crystals
3D	Three-Dimensional
3DPC	Three-Dimensional Photonic Crystal
BB	Blackbody
EQE	External Quantum Efficiency
EWFD	Electromagnetic Waves, Frequency Domain
FEM	Finite Element Method

FSS	Frequency Selective Surface
GHGs	Green House Gases
NREL	National Renewable Energy Laboratory
NP	Nanoparticle
P	Porosity
PV	Photovoltaic
PC	Photonic Crystal
TEGS	Thermal Energy Grid Storage
TPV	Thermophotovoltaic

# 1 Introduction

In today's world, finding new and efficient ways to create renewable energy is a top priority for researchers. One exciting development in this area is the rise of TPV systems. These systems are gaining attention because they offer a fresh approach to using heat energy, turning it directly into electrical power. At its core, TPV technology is a game-changer because it directly converts radiant heat from a high-temperature object into electricity using a photovoltaic (PV) cell. Thermal energy from a high temperature heat source is used to elevate the temperature of an emitter, and the radiation it emits is converted to electric power in a PV cell (Figure 1). TPV holds the potential to transform the power generation landscape across numerous sectors, offering a solution that is environmentally friendly, durable, and efficient for electricity production.

This introduction aims to give you a clear understanding of how TPV systems work and why they could be a significant step forward in renewable energy research. I hope to spark your interest as this thesis dives deeper into the fascinating world of TPV systems in the upcoming sections.

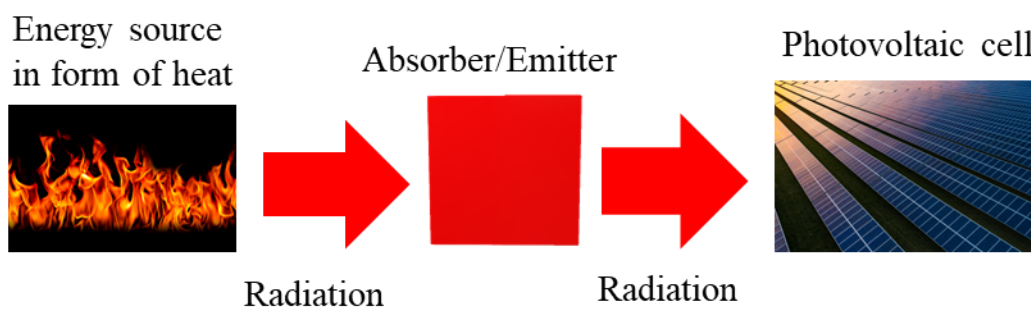


Figure 1. TPV energy conversion

## **1.1 Global Warming**

The accelerated growth of human activities has led to an increased release of greenhouse gases (GHGs) into the atmosphere, causing global warming. The results of this are far-reaching, from rising sea levels to more frequent and severe natural disasters.

## **1.2 Energy Production Globally and in Canada**

Coinciding with the rise in global temperatures is the world's ever-increasing appetite for energy. With industrialization and modernization, dependence on fossil fuels, the prime contributors to GHGs, has become evident, calling for urgent diversification and optimization of energy sources. Figure 2 illustrates the trend in global primary energy consumption from various sources between 1965 and 2022, as indicated in reference [1]. The data reveals a consistent increase in energy consumption, nearing 160,000 TWh. Despite the significant contribution of fossil fuels to this total, renewable energy sources have not yet scaled up sufficiently to provide a substantial competition to these traditional energy technologies in global scale.

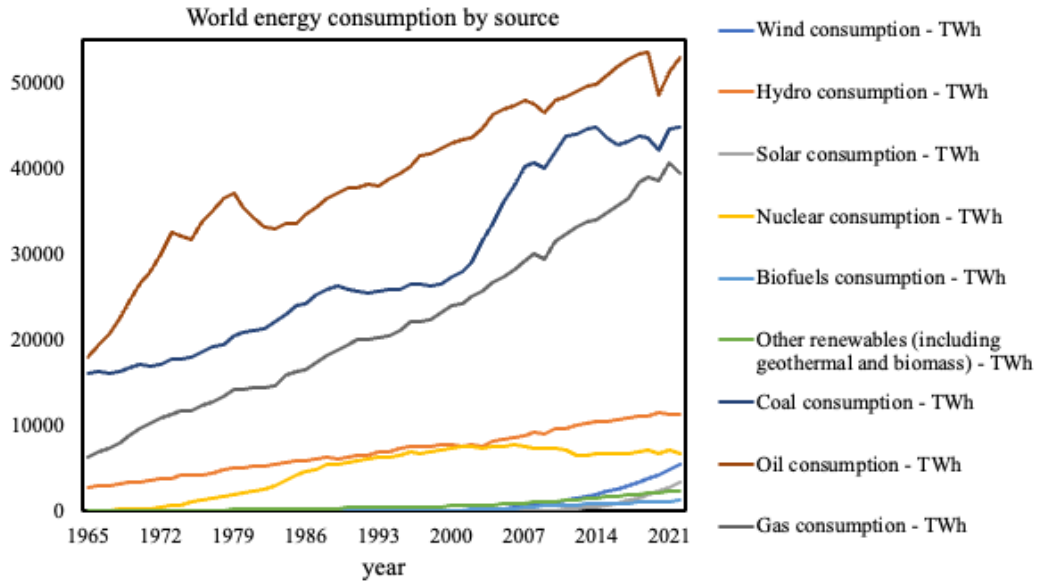


Figure 2. Global primary energy consumption from different resources [2]

Enacted on June 29, 2021, the Canadian Net-Zero Emissions Accountability Act solidifies Canada's pledge to transition from fossil fuels to renewable energy, targeting net-zero emissions by 2050 and promising government transparency and accountability in reaching this goal [3].

Figure 3 illustrates Canadian energy consumption by sources, demonstrating that hydro as a renewable source play an important role while solar and wind are still minimal. Canada prioritizes hydroelectric power in its energy portfolio due to abundant water resources, providing a clean, reliable, and economically beneficial source that aligns with the country's commitment to sustainable energy and regional development. The strategic emphasis on large-scale hydro projects contributes significantly to Canada's diversified energy mix and enhances overall energy security.

Canada is at the vanguard of this global shift, dedicating efforts to foster and enhance technologies that make renewable energy sources more affordable, efficient, and long-lasting.

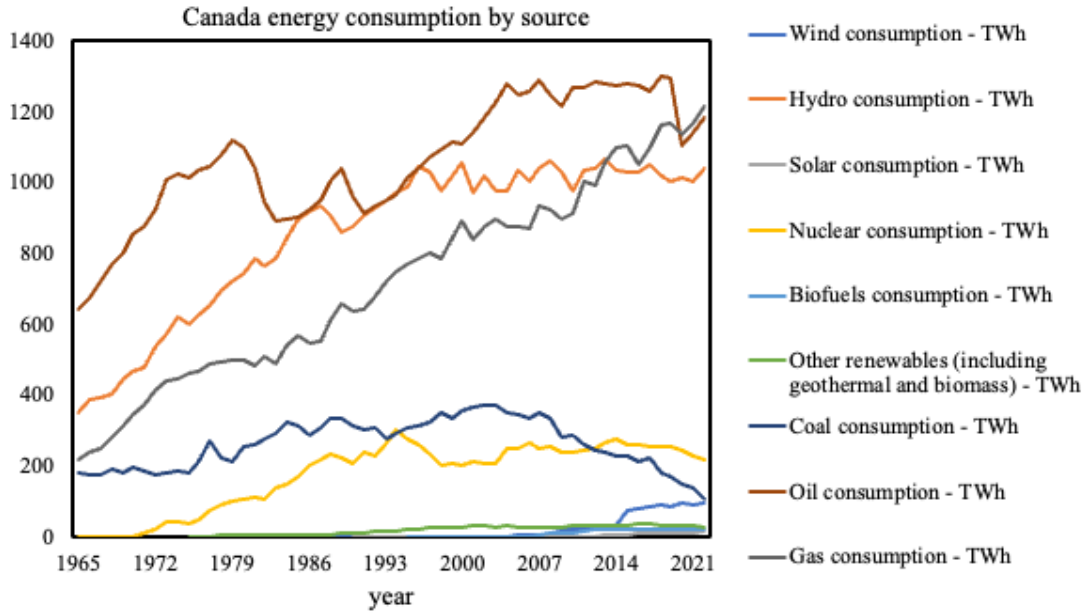


Figure 3. Canada energy consumption by source [2]

### 1.3 Renewable Energy Resources

In response to the environmental crises, there's been a pivot towards renewable energy resources. Solar, wind, and hydroelectric power have emerged as frontrunners in this transition, contributing to a sustainable and cleaner energy future. However, these sources of energy have their own sets of challenges. Hydroelectric power is not available everywhere, and solar and wind energies are dependent on specific weather and time conditions.

It is practical to combine renewable energy systems with a backup that runs on fossil fuels or biomass. Another innovative method is storing extra energy as heat when available and using it when resources are low. Recently, the important role of TPV in transitioning to clean energy has been recognized, as research has increasingly been directed toward the optimization of TPV systems.

## 1.4 History of Thermophotovoltaic

TPV has played a pivotal role in energy conversion since its inception in the mid-20th century. Historical records often attribute figures like Dr. Pierre Aigrain [4], [5] and Henry H. Kolm [6] with the early development of TPV systems. Henry H. Kolm in 1956, [7] with his innovative setup, combined a camping lantern with a silicon PV cell. In the initial years, TPV systems predominantly relied on fossil fuels as heat sources. In 1963 John J. Worth patented the pioneering TPV converter designed to harness heat from engine exhausts [8]. In the 1970s, due to the energy crisis, researchers were prompted to explore alternative heat reservoirs for TPVs [9], [10]. Fast forward to the 1990s, the initial National Renewable Energy Laboratory (NREL) TPV conferences underscored the urgency of actionable strategies to enhance TPV's overall efficiency [11], [12]. The subsequent years witnessed a surge in technological innovations and entrepreneurial endeavors in the field of TPV.

Recent advances in TPV underscore its growing significance. Pioneering startups include Antora Energy (2018), focusing on zero-carbon heat through innovative thermal batteries (Figure 4) [13], and Mesodyne's LightCell™ (2018) utilizes micro combustors to heat nanophotonic materials, efficiently generating power and bridging the energy gap between batteries and combustion engines, with adaptability to various fuels and low maintenance [14]. Similarly, Thermophoton (2021) emphasizes Power-to-Heat-to-Power storage, offering a cost-effective alternative to Li-ion batteries by storing electricity as heat [15]. On the academic side, TPV-13 and TPV-14 conferences showcased the breadth of TPV innovations. Notably, TPV-14 brought forward cutting-edge research from global institutions. TPV-13 conference delved into tailored spectral thermal

emission techniques, high-temperature emitters, near-field TPV and diverse TPV applications [16]. Meanwhile, TPV-14 emphasized on empirical TPV design, integrated TPV system, novel emitter designs and bifacial TPV concept drawing experts from renowned global institutions [17].



Figure 4. Antora Energy’s battery running at a facility in Fresno, California [18]

## 1.5 Applications of thermophotovoltaic

TPV energy conversion offers a promising avenue in harnessing radiant energy. It relies on the conversion of thermal energy to electricity by capturing the radiation emitted by a thermal emitter using PV cells. Its applications are diverse, spanning from industrial waste heat recovery [19], solar TPV [20], [21] , thermal energy grid storage (TEGS) [22], [23], portable generators, uninterruptable power supplies, self-powered heating devices and power generation in space [24]–[27]. In this thesis, I am targeting to optimize TPV systems for TEGS.

### **1.5.1 Thermal Energy Grid Storage**

In grid storage systems utilizing TPV technology, electrical energy is converted into thermal energy and preserved within well-insulated, economically viable graphite blocks. This system, designed to operate optimally with renewable energy sources, channels surplus electricity into a transformation process facilitated by refractory heating elements characterized by their high resistance properties.

These graphite blocks act as efficient reservoirs, holding the converted thermal energy until a demand for electricity arises within the grid. At the point of discharge, the heat harbored within the graphite is mobilized to power a heat engine, thereby converting the stored thermal energy back into electrical power. This process exemplifies a renewable-friendly approach to energy storage and management, leveraging the potential of TPV technology in advancing sustainable energy solutions.

In the context of TPV technology for TEGS, the process is relatively straightforward: excess electricity, particularly from renewable sources, is turned into heat using high-resistance elements. This heat is then stored in affordable, insulated graphite blocks [Figure. 5].

When the demand for electricity arises, the stored heat within the graphite is released to power a heat engine, which then generates electricity to meet the demand. This cycle showcases an efficient and eco-friendly way to store and reuse energy from renewable sources, making the most of their potential while providing a reliable power supply.

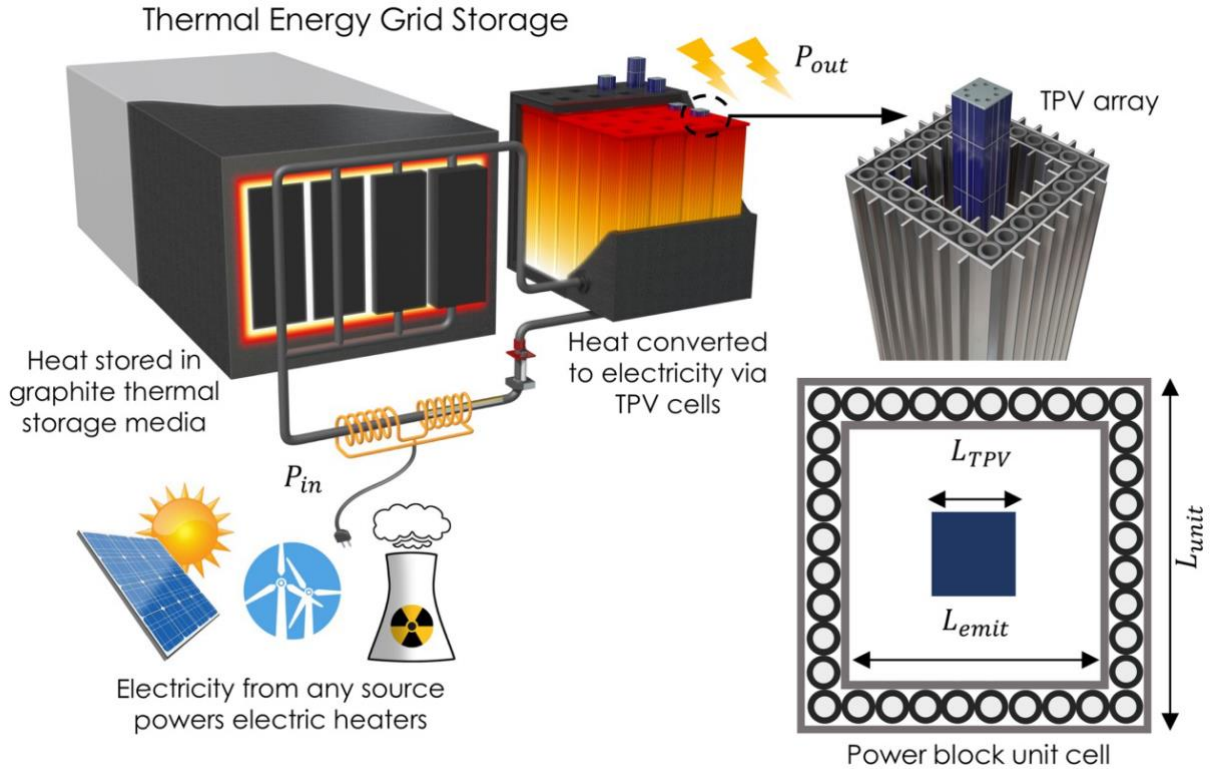


Figure 5. The concept of thermal energy grid storage system using TPV (Reprinted with permission from Ref.[28], Springer Nature)

Initially, the development of Thermal Energy Grid Storage (TEGS) focused on utilizing molten silicon as the primary storage medium [29]. However, a transition to a graphite storage medium has proven to be more economical, costing approximately US \$ 0.5 per kilogram. Consequently, the anticipated capital expenditure per unit of energy (CPE) is projected to be under US \$ 10 per kWh [30].

Remarkably, this reduced cost structure not only meets but potentially undercuts the outlined cost objectives (less than US\$20 per kWh) set for long-term energy storage systems. As a result, this positions TEGS as a viable contender in making renewable energy accompanied by storage solutions a financially competitive alternative to traditional fossil fuel-based power sources, as detailed in references [30]–[32].

## 1.6 Research Gaps

Despite the considerable potential of TPV systems in renewable energy applications, there remains a consistent obstacle concerning the spectral and directional control of thermal radiation that reaches the PV cells [33], [34]. One viable strategy for mitigating this issue involves employing photonic crystals (PC) as an optical filter.

In this study, the possibility of enhancing the in-band transmission of 1DPC filters with graded refractive index profiles is explored. Previous research by Southwell highlighted that the transmission at an interface can markedly increase when the refractive index profile at that interface follows a quintic function, allowing for a gradual transition from low to high refractive index across the boundary [35]. Past studies have numerically demonstrated that 1DPCs with such refractive index profiles at their internal boundaries can boost the efficiency of transparent windows in parabolic dish concentrator receivers [36], [37]. The prospective advantages of utilizing Rugate filters in TPV systems have been noted as well [38]. Yet, as far as the author is aware, there are no published papers on the use of 1DPC filters with graded refractive index profiles at their internal boundaries in TPV systems. In this study, numerical analyses is carried out to ascertain the reflection and transmission spectra of 1DPC TPV filters that have internal boundaries characterized by a quintic function-graded refractive index profile.  $\text{ZrO}_2$  and  $\text{SiO}_2$  NP films for the high and low refractive index layers within the 1DPC are selected, respectively, owing to their high transparency and minimal absorption characteristics.

This study aims to delve deeply into the functionality of 1DPCs with graded structures [39], contrasting them with quarter-stack [40] and modified quarter-stack [41] configurations. The overarching goal is to optimize these structures explicitly for TPV applications, thereby potentially elevating the overall efficiency and electrical power output of TPV systems.

## 1.7 Objective

The primary goal of this thesis is to conduct a thorough analysis of 1DPCs, with a focus on investigating the effects of grading their refractive index profile and how the effects their performance when functioning as optical filters in TPV systems. objectives are stated below:

- Study the effect of a graded index of refraction on the transmission, reflection, and absorption of 1DPC filter.
- Design 1DPC with graded index of refraction profile to function as optical filter in TPV system.
- Compare the effects of graded index of refraction profile of 1DPC filters on the performance of TPV system in terms of power output and TPV efficiency.

To meet the objectives listed above, a numerical approach will be utilized:

Numerical Model: A numerical model will be developed using COMSOL to analyze the optical behavior of 1D  $\text{ZrO}_2/\text{SiO}_2$ -NP PCs in quarter-wave stack, modified quarter-wave stack, and graded structures.

Theoretical Model: In addition, a theoretical model will be created for the TPV system which includes components such as a BB emitter, 1DPCs functioning as the optical filter, and a GaSb PV cell.

This combined approach aims to provide a comprehensive understanding and viable optimization pathways for TPV systems incorporating 1DPCs.

## **1.8 Overview**

The structure of this thesis is laid out as follows:

An introduction to TPV is given in Chapter 1. This chapter traces the history of TPV, explores its diverse applications, particularly in TEGS, and addresses global challenges like climate change. The research aims to bridge gaps in TPV systems, proposing innovative solutions for more efficient and sustainable energy conversion.

Background pertaining to TPV systems is provided in Chapter 2, which provides a thorough overview of TPV system, covering components, spectral control, and literature review for optical filters. It introduces spectral and directional control with an optical filter. The role of the BB emitter and the significance of PV cells, especially GaSb, are discussed. Spectral control with front cold side filters is explored. The introduction of 1DPCs and their efficiency in TPV systems is highlighted. The optical properties of NPs and their preparation methods are briefly discussed.

Chapter 3 discusses the methodology used to carry out the numerical simulations presented within this thesis. A comprehensive methodology to investigate TPV systems with a focus on a planar emitter, GaSb PV cell, and a 1DPC acting as a selective filter. Six distinct 1DPC filters, featuring structural arrangements such as quarter-wave, modified quarter-wave, and graded indices stacks,

are analyzed for their impact on system performance. The study incorporates material properties of SiO<sub>2</sub> and ZrO<sub>2</sub> NPs, exploring optical properties and optimizing TPV efficiency. The methodology integrates the Stefan–Boltzmann law, Planck's law, and various equations for parametric analysis and exploring the impact of in-band transmission and out-of-band reflection on TPV efficiency, providing insights into filter performance. Additionally, this numerical study incorporates the Wave Optics Module in COMSOL Multiphysics, utilizing the FEM to analyze electromagnetic wave behavior in optical structures, particularly PCs, offering a versatile platform for optimizing optical component performance and exploring complex 1DPCs designs.

The results from this research are presented in Chapter 4. Notably, a dual-stack graded filter, at 2000 K emitter temperature, achieves 74% in-band transmittance and 55% out-of-band reflectance, while the dual-stack modified quarter-wave stack shows 64% out-of-band reflectance and 70% in-band transmittance. Efficiency and power metrics set benchmarks, highlighting the challenge of balancing in-band transmittance and out-of-band reflectance. The thesis concludes that optimal filter structures involve dual filters with varied peak positions and a modified quarter-wave stack profile. Implemented in an ideal TPV system, acting as a photon recycling apparatus, this optimized filter yields 24% system efficiency and 6.9 W/cm<sup>2</sup> power density.

Chapter 5 presents a discussion of the results from this research. This chapter explores the challenges and emerging methods for fabricating graded-index profiles in optical filters for industrial-scale TPV systems. While acknowledging the current economic limitations of the introduced optical filters, the discussion highlights recent advancements, such as oblique-angle deposition, for achieving precise graded index profiles. The need for practical and cost-effective fabrication methods is emphasized, and future work is proposed to leverage emerging techniques. The chapter also employs a theoretical approach, disregarding absorption to examine the effects

of in-band transmission and out-of-band reflection on TPV system efficiency. Plots are presented to visualize the impact of optical parameters, providing a "map" for improving spectral and TPV system efficiency. Additionally, a comprehensive table compiles numerical and experimental studies on TPV with 1DPC optical filters, detailing PV cell and emitter temperatures, spectral efficiency, power output, and other relevant parameters for comparison.

The conclusions from this work are stated in Chapter 6. In summary, this study addresses the persistent challenge of controlling thermal radiation in TPV systems and focuses on improving in-band transmission using 1DPC filters with graded refractive index profiles. The objectives involve conducting a comparative study of 1D PC graded structures, developing optimization strategies for TPV systems. The thesis structure includes sections on TPV introduction, design, simulation, and validation of the proposed PC optical filter, and performance analysis. Noteworthy findings include promising results from a dual-stack graded filter and the potential of an optimized filter structure with a modified quarter-wave stack profile for photon recycling. These insights contribute to understanding the limitations of TPV systems and its optimization.

## 2 Background

In the preceding chapter, the TPV system, its application, as well as the research question and objective of this thesis were presented. The current chapter furnishes an overview of background knowledge necessary for comprehending the methodology and results, accompanied by a literature review on the subject.

### 2.1 Thermophotovoltaic Systems

TPV directly converts radiant heat from a high-temperature object into electricity using a PV cell.

TPV systems [Figure 6] have two main components: an emitter and a PV cell.

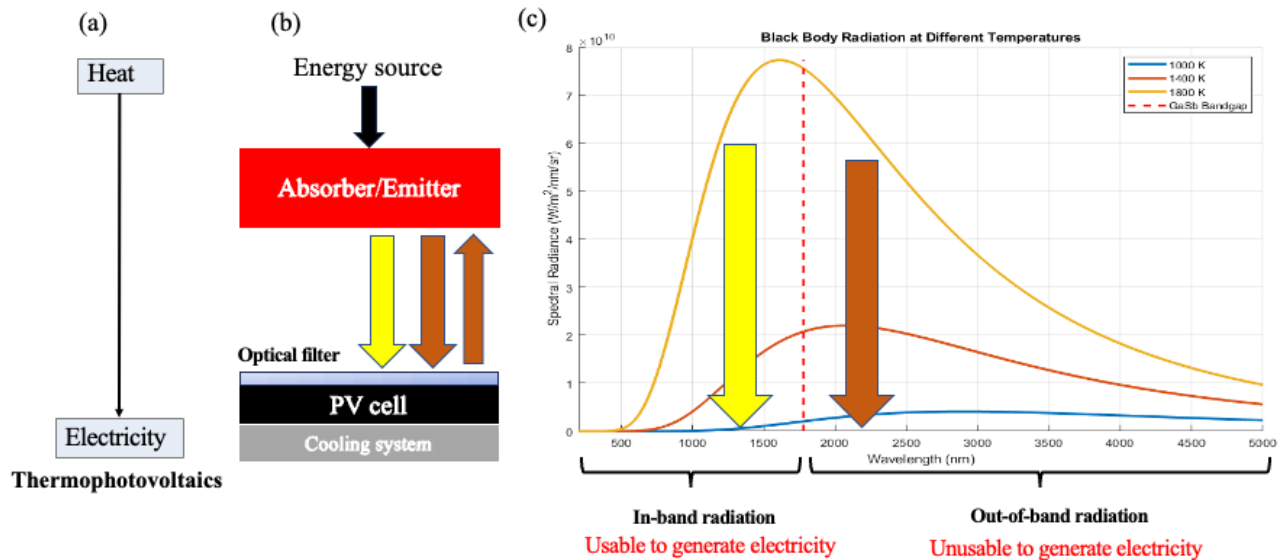


Figure 6. TPVs system: (a) Energy conversion in TPVs, (b) Schematic of a TPV system with an optical filter placed on top of the PV cell, (c) Concept of radiation spectrum, bandgap, and BB radiation in TPVs.

Some of the radiation emitted from the hot surface of the emitter is captured by PV cells and converted into electric power. The remaining portion is lost in the system. Emitter radiation possesses both spectral and directional properties, meaning its intensity varies in different wavelengths and incident angles. PV cells can only generate electricity using incident light within a specific wavelength range known as in-band radiation. They are incapable of generating electricity outside this range, referred to as out-of-band radiation [Figure 6, c]. Additionally, PV cells exhibit an angle-dependent property, producing electricity more effectively at angles close to normal and less efficiently at higher angles.

An optical filter, positioned between the emitter and PV cell, is used to control the radiation reaching the PV cell in terms of both spectral and directional characteristics. An ideal optical filter reflects out-of-band radiation while allowing in-band radiation to pass through [Figure 6, b]. This filter acts as a photon recycling tool to increase the emitter's temperature, and reducing energy loss in the PV cell.

The PV cell in a TPV system operates under conditions distinct from those of a PV cell exposed to sunlight. In a TPV system, the PV cell typically functions in a high view factor environment because the emitter is positioned in close proximity. This is in contrast to sunlight, which comes from a considerable distance. In TPV systems, a significant portion of the light falls within the out-of-band range. This underscores the importance of having an optical filter capable of reflecting this out-of-band light without impact on the in-band radiation.

### 2.1.1 Emitters in Thermophotovoltaic

An effective emitter for a TPV system should have a high radiative emissivity for in-band photons, which can be converted by the PV cell, and a low emissivity for out-of-band radiation. A BB emitter fulfills the first requirement but has to be operated together with a selective filter to account for the second one. A selective emitter in principle can fulfill both requirements at once. Different approaches to design selective emitters were published in the literature.

Selective emitters [42] suppress the emission of longer wavelength photons with energy less than the bandgap of the PV cell (referred to as out-of-band photons) while enhancing the emission of photons with energy above the bandgap of the PV cell (referred to as in-band photons). One approach to design selective emitters is to structure them in the form of one-dimensional (1D) [43], [44], two-dimensional (2D) [45], [46], or three dimensional (3D) [47]–[49] photonic crystals (PCs) [50]. However, PC emitters operate at temperatures typically higher than 1200 K over many cycles and their structure undergoes thermal degradation.[51]–[53] .

In TPV systems, the BB emitter holds a pivotal role in the energy conversion process, functioning as a theoretical entity that absorbs all incident electromagnetic radiation, and re-emitting it as BB radiation, characterized by a temperature-dependent emission spectrum described by Planck's Law. In this study, the BB emitter is used as a standard tool to help test and improve the effectiveness of new filter designs in the TPV system. This process helps us to better understand how to control and direct IR radiation in TPV systems, potentially leading to new developments in green energy solutions.

### 2.1.2 PV cells in Thermophotovoltaic Systems

In TPV systems, the PV cell plays a crucial role in converting radiant energy into electrical power.

This cell consists of several main components [Figure 7]:

**Absorber Layer:** The core part where thermal radiation is absorbed, primarily composed of a semiconductor material that forms a p-n junction, facilitating the conversion process.

**P-N Junction:** A critical area within the absorber layer where p-type (positive) and n-type (negative) semiconductors meet, creating an electric field that helps in generating an electric current.

**Anti-Reflective Coating:** A layer applied to the cell's surface to enhance radiation absorption and reduce energy losses due to reflection.

**Electrical Contacts:** These are present on the front and back of the cell, enabling the extraction and flow of the generated electrical current to an external circuit.

**Encapsulation:** This protective layer shields the PV cell from environmental factors, ensuring durability and long operational life.

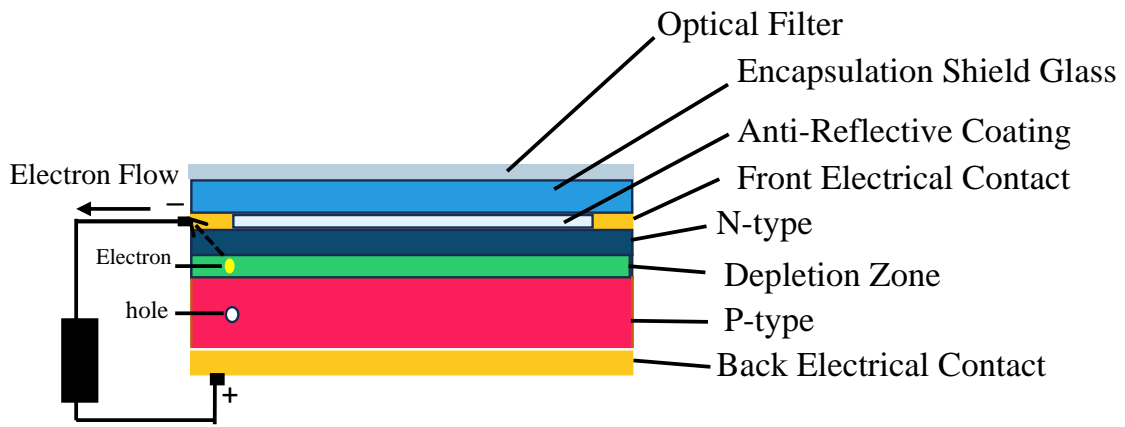


Figure 7. Schematic of PV cell for TPV application equipped with an optical filter.

The PV cell in a TPV system is typically tailored to have a high conversion efficiency for the specific spectral radiations emitted by the emitter, optimizing the overall efficiency of the system. It is crucial for the PV cell to be matched with the emitter's spectral properties to enhance the TPV system's performance.

PV cells are commonly constructed from semiconductor materials. Their performance tends to decline as the temperature rises, largely due to the enhanced recombination rates of internal carriers, a result of increased carrier concentrations. One notable impact is a decrease in the bandgap of the semiconductor material, which in turn affects various semiconductor properties. Essentially, as temperature increases, the energy level of electrons within the material also rises. This means that it takes less energy to break the bonds holding electrons in place.

In a semiconductor's bond model, a reduction in bond energy leads to a reduction in the bandgap. So, increasing the temperature ultimately lowers the bandgap, which reduces the open-circuit voltage ( $V_{oc}$ ). On the other hand, the short-circuit current ( $I_{sc}$ ) experiences a slight increase with rising temperature. This occurs because the lower bandgap energy allows more photons to possess sufficient energy to create electron-hole pairs. However, this effect is relatively small [54].

Researchers focused on developing low bandgap PV cells for TPV applications. Different semiconductor materials are used in fabricating TPV cells including Ge [55] , Si [56], InGaAs/InP [57], GaSb [58] , InGaAsSb [59], AlGaAsSb [60], InAsSbP [61] and InAs [62]. GaSb with a bandgap of 0.72 eV, TPV cells are often considered the best fit for contemporary TPV system due to their efficiency and simplicity of the diffusion technology employed [63].

Nevertheless, for TPV cells with bandgaps lower than that of GaSb, they may have an edge when paired with low-temperature TPV systems that don't selectively filter wavelengths, as these cells can better capture the infrared radiation emitted by a BB. In this study, the performance of the proposed 1DPC filter paired with a GaSb PV cell will be examined.

### **2.1.3 Spectral control in Thermophotovoltaic Systems**

Control of radiation from the emitter is an important aspect of advanced TPV systems [33], [64], as it determines the degree of thermalization losses in the PV cell, and the PV cell temperature. Common components used to control the emission and reflectance of radiation in TPV systems include selective emitters [65], back surface reflectors (BSRs) [66], [67], and cold side filters [68]. BSRs are metallic layers of Au [27], [28] or Ag [70] at the rear side of the PV cells. BSRs reflect both in-band and out-of-band photons. In-band photons reflected by the BSR have a second chance to be absorbed in the PV cell, while out-of-band photons reflected by the BSR can return to and be absorbed by the emitter. BSRs significantly improve the performance of TPV systems. However, even with the integration of highly efficient BSRs a significant number of out-of-band photons are absorbed at the rear side of the PV cell. This parasitic absorption has the dual disadvantage of increasing optical losses and increasing the temperature of the PV cell [69], [71], [72]. Front side cold filters can be used to significantly reduce the amount of out-of-band radiation absorbed in the PV cell. These filters are used near the front surface of the PV cell, which typically operates between 25 °C and 45 °C. Front cold side filters are highly transmissive for in-band photons and highly reflective for out-of-band photons. Radiation reflected by the cold side filter can be absorbed by the emitter which reduces optical losses, elevates the temperature of the emitter, and increases the efficiency of the TPV system.

#### 2.1.4 Front Cold Side Filters

Different front side filters in TPV systems have been explored in previous studies. Kristensen et al [73] expanded the application of frequency selective surface (FSS) technology, commonly utilized in the microwave band, to be applicable in the near-infrared spectrum for use as a filter in TPV systems. But the application is hindered by ohmic losses in the metallic FSS, restricting their efficiency in TPV systems.

Additionally, Höfler and team [74] studied Ag/SiO<sub>2</sub> filters and noted that these filters could attain a reflectance of about 96% at normal incidence. This, however, came with a drawback of significantly reducing the amount of valuable radiant power that is transmitted to the PV cell.

Demichelis and colleagues [75] introduced a filter designed with a dielectric-metal-dielectric structure. This structure incorporates a slim 20 nm silver layer situated between two dielectric layers made of ZnS (with a refractive index of 2.32) and MgF<sub>2</sub> (with a refractive index of 1.38). This proposed filter demonstrates more than 85% light passage in a wavelength range from 0.85 μm to 1.15 μm, making it a good match for Ge PV cells.

Research has been conducted into using patterned amorphous silicon layers on quartz bases as filters for TPV systems. The findings indicate that 72% of the radiation that falls outside the desired bandwidth (more than 1.80 μm) can be 'recycled', as it gets reflected back towards the absorber[76].

Plasma filters [77], which are essentially densely doped semiconductor layers functioning to selectively manage the reflection or transmission of specific thermal radiation frequencies, have been studied in the context of reflecting long wavelengths for TPV applications.

Rahmlow et al. [51], [78] discussed the functioning of plasma filters when they are paired with interference filters in TPV systems. The plasma filter is engineered to reflect longer wavelengths, whereas the interference filter targets wavelengths close to the PV cell's bandgap. These interference filters have the ability to reflect nearly the entirety of radiation spectrum in the specific wavelength range. In a related development, Vigil adjusted the free electron concentration and the thickness of layers in the transparent conducting oxide (TCO), specifically ( $\text{SnO}_2\text{:F}$ ) to use it as an effective filter in a TPV system [79]. Numerous studies have explored the role of PC structures as filters for TPV systems, a topic that will be further detailed in the following section.

## 2.2 Photonic Crystal

Definition of Photonic Crystals (PCs): PCs are structures made up of layers of materials that alternate in their refractive indices. These can be found in one-dimensional (1D), two-dimensional (2D), or three-dimensional (3D) forms, each having its own unique properties and applications [Figure. 8]. This section will introduce the various forms of PCs and explain their different structural characteristics. In a simple 1DPC, you might have layers of two materials with different refractive indices, referred as H (high-index) and L (low-index). When light encounters this periodic structure, it can either be transmitted or reflected depending on the light's wavelength and the photonic crystal's structure.

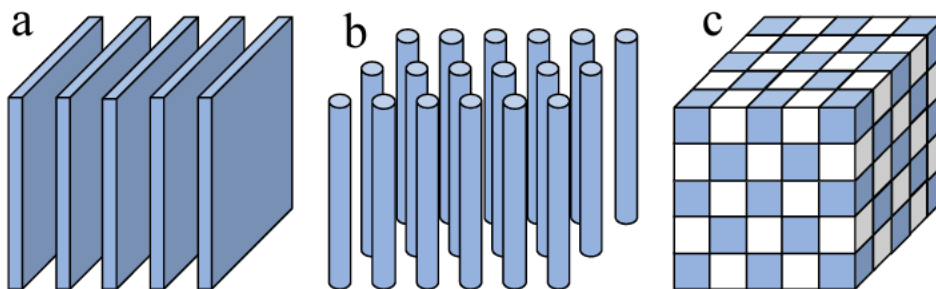


Figure 8. Structural variations of PCs: (a) 1D, (b) 2D, and (c) 3D configuration.

Concept of photonic bandgap: A band gap is a range of frequencies (or wavelengths) over which light cannot propagate through the crystal. This occurs because, at certain frequencies, the interference of light within the photonic crystal is completely destructive, meaning that any incoming light at those frequencies is reflected instead of transmitted. The result is a gap in the spectrum where the crystal appears to be perfectly reflective, and no modes of light can propagate through the crystal.

In 1DPCs, even a small contrast in the refractive index between the two alternating layers can result in a complete photonic band gap or stop gap. This is because, in 1DPC even small periodic changes in the refractive index can be enough to cause the necessary destructive interference for forming band gap formation (Figure 9, a). However, when moving to 2DPC (Figure 9, b) or 3DPC (Figure 9, c), achieving a full photonic band gap becomes more challenging. This is due to the more complex ways in which light can propagate and interfere within the structure. In these higher-dimensional systems, light has more paths to navigate through the crystal, which means that more substantial index contrasts are required to ensure that destructive interference occurs across all possible paths, leading to a full band gap. This necessitates a careful design of the photonic crystal's geometry and material properties to tailor the band gaps effectively for using these structures as an optical filter.

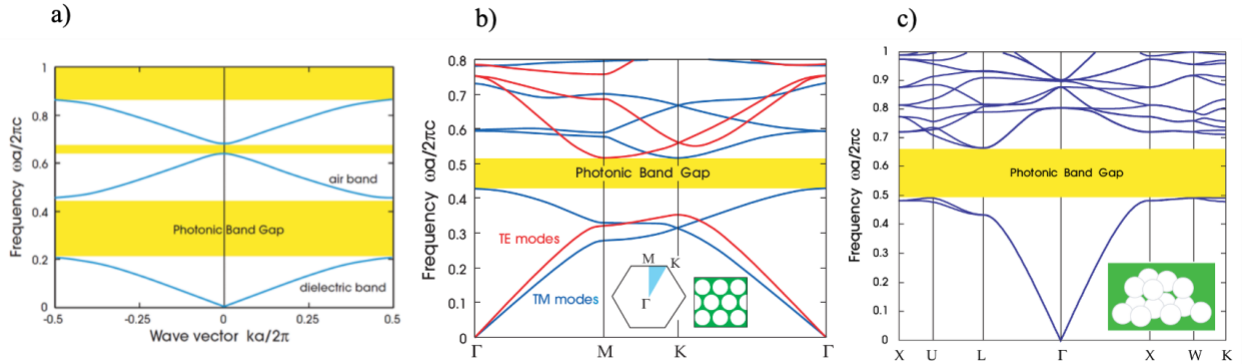


Figure 9. Photonic band diagram for a) 1DPC, b) 2DPC and c) 3DPC (Reprinted with permission from Ref. [80], The Princeton University Press)

Effects of Layer Thickness on 1DPC: In a 1DPC, the thickness of layers is a critical factor that determines the behavior of light within the crystal. Lattice constant is the spatial period of the crystal, in other words, the thickness of one cycle of the two materials. If you increase the thickness of the layers, you're essentially stretching the period of this interference pattern, which can shift the band gap to longer wavelengths (lower frequencies). Conversely, decreasing the thickness shifts the band gap to shorter wavelengths (higher frequencies).

Effects of index of refraction on 1DPC: The material properties, specifically the permittivity ( $\epsilon$ ), also influence the band gap. The dielectric function relates to how a material polarizes in response to an electric field and, therefore, its refractive index. Increasing the difference in the permittivity or equivalently, the refractive indices of the two materials amplifies the contrast between layers in terms of how they interact with light. A greater contrast means that the difference between how the two materials reflect and transmit light is more pronounced, leading to stronger destructive interference and thus, a wider band gap. This wider gap means a broader range of frequencies where light cannot propagate, which is often desirable in applications like optical filters or waveguides, where you want to precisely control which wavelengths of light pass through.

In theory it is assumed that in a 1DDPC structure periodicity is in one direction and in the two other direction it goes to infinity. however, in practice 1DPC have limited dimension and some light will be transmitted through the photonic crystal over the bandgap region.

When a L material layer is positioned at the beginning of a one-dimensional photonic crystal, creating a structure denoted by  $L[HL]^P_{\lambda_0}$ , it yields a reduced reflectance. This occurs as an incident wave from the air initially encounters a L material at the interface. Conversely, in a structure represented by  $H[LH]^P_{\lambda_0}$ , the incident wave from the air first interfaces with a H material which increases reflectance due to a wider photonic bandgap.

### 2.2.1 One-Dimensional Photonic Crystals

The simplest form of PCs is One-dimensional photonic crystals (1DPCs), where the periodicity in the refractive index occurs along one dimension (Figure 8, (a)). These can be found in coatings and filters that reflect or allow certain types of light to pass through, depending on their design and the materials used [36], [40], [81]–[84], [84], [85], [85], [85], [86], [86], [87]. 1D PC consists of periodic layers of low (L) and high (H) indices of refraction.

The structure of 1DPC filters can be presented using a notation wherein L present a layer with low index of refraction and H represent a layer high index of refraction. For example, in  $H[LH]^P_{\lambda}$ , the sequence of layer starts from left to right with the H layer. Then, P represents the number of times the [LH] layers are repeated and  $\lambda$  is the reflectance peak wavelength position, which will be explained later in the methodology section.

It has been recognised that PCs can function as high-performance filters in TPV systems. The reflectance and transmittance spectra of PCs can be tuned by designing the periodicity of their index of refraction profile. PC filters for TPV systems can be made from highly transparent

materials that exhibit minimal absorption over the wavelength region of interest. Mostafa et. al. investigated a 1DPC filter comprising Ag/SiO<sub>2</sub> layers. It was assumed the thickness of the Ag layers were much less than their skin depth of 12 nm. Their numerical analysis showed the effective transmission for in-band radiation is around 78%. Celanovic et. al [40], [41] utilized amorphous silicon (Si) and SiO<sub>2</sub> to create a dielectric-dielectric multilayer PC structure. They fabricated Si/SiO<sub>2</sub> filters with broad reflectance peaks using low-pressure chemical vapor deposition with (LH)<sup>5</sup> and L/2H(LH)<sup>4</sup> configurations. Further, by reducing the thickness of the first layer in the quarter-wave stack by half the transmission of in-band photons was improved, resulting in a spectral efficiency of 40% and integrated in-band transmission of 65% at 1500 K [83]. Liu et al. [84] fabricated a 1DPC filter with Si/SiO<sub>2</sub> layers arranged in L/2 H (LH)<sup>3</sup> and (LH)<sup>4</sup> configurations, and achieved a spectral efficiency of 46%. Mao and Ye [85] aimed to minimize pass-band oscillations in the wavelength range of 1.45–1.75 μm by modifying the Si/SiO<sub>2</sub> 1D PC structure. They proposed a  $(1+\Delta_1)(L/2HL/2) (L/2HL/2)^3 (1+\Delta_2)(L/2HL/2)$  configuration and recommended  $\Delta_1$  and  $\Delta_2$  values between 0.08–0.12 and 0.06–0.16, respectively. This modified structure achieved a spectral efficiency of 55.2% for an emitter temperature of 1800 K. Babiker et. al. [88] fabricated a 1D Si/SiO<sub>2</sub> PC filter using magnetron sputtering. They subsequently analysed the influence of incidence angle and the number of periods on spectral reflectance. Their results from simulations indicated a spectral efficiency of 33.5% for the modified structure at an emitter temperature of approximately 1500 K. Mbakop et. al. investigated the potential of using a one-dimensional TiO<sub>2</sub>/SiO<sub>2</sub> PC filter for TPV applications [89]. Their results showed that broad reflectance peaks with sharp cut-off edges could be achieved for TiO<sub>2</sub>/SiO<sub>2</sub> filters comprising six periods.

Another study [90] showed that the side reflection ripple in TiO<sub>2</sub>/SiO<sub>2</sub> structures were smaller than those in Si/SiO<sub>2</sub> structures. The Si/SiO<sub>2</sub> structures were found to have a wider bandgap compared

to the  $\text{TiO}_2/\text{SiO}_2$  structures. The investigation of the  $\text{TiO}_2/\text{SiO}_2$  1D PC with a structure layer of  $(\text{LH})^p(\text{LL})(\text{HL})^p$  and  $(\text{LH})^p$  showed that the TE polarization transmission spectrum shifted significantly towards smaller wavelengths when the period increased from  $P=6$  to  $P=8$ . In contrast, the shift was gradual for the TM polarization. The forbidden band becomes narrower when the incident angle of the light is  $25^\circ$  [86]. Khosroshahi [91] proposed a loss mechanism for 1DPC  $\text{Si}/\text{SiO}_2$  optical filters in TPV systems. His simulation considered the spectral refractive and absorptive indices of both materials. He also stacked a similar structure on top of the first filter to minimize loss due to above band-gap incident radiation to less than 10% at 1800 K. A numerical investigation was conducted on 1DPC made of  $\text{Ge}/\text{MgF}_2$  material, demonstrated spectral efficiency of 75%. The  $\text{MgF}_2$  layers remain transparent across the entire wavelength range of interest, and absorption is mainly attributed to the Ge layers. The absorptance curves are directly correlated to the extinction coefficient of Ge [92]. A 1D PC structure was created by interchanging layers of titanium dioxide ( $\text{TiO}_2$ ) and graphene oxide (GO), exhibiting a spectral efficiency of 64% at a source temperature of 1800 K [82]. The investigated high refractive index materials were found to be absorptive. A proposed one-dimensional PC made of  $\text{ZrO}_2/\text{SiO}_2$ -aerogel [35] with a nanoporous structure was found to have a low absorption index in the range of  $10^{-6}$  to  $10^{-2}$  for wavelengths between  $0.3 \mu\text{m}$  to  $8 \mu\text{m}$  [81].

### 2.2.2 Two-Dimensional Photonic Crystals

Two-dimensional photonic crystals (2DPCs) are more complex, having variations in refractive index along two different axes (Figure 8, b). This allows for more intricate control of light, making them useful in devices such as waveguides and beam splitters that guide or split light beams in certain ways [93].

### **2.2.3 Three-Dimensional Photonic Crystals**

Three-dimensional photonic crystals (3DPCs) are the most complex type, with periodic variations in the index of refraction occurring in three different directions (Figure 8, b). These crystals can control light in more complete ways, which makes them promising for creating highly efficient devices like light-emitting diodes or solar cells [94] that can absorb more light. However, making these 3D structures is quite challenging because of their complexity [95].

## **2.3 Optical Properties of Nanoparticles**

nanoparticles (NPs) are particles with dimensions up to 100 nm. These particles often exhibit unique characteristics distinct from larger-scale substances. Due to their versatility, NPs find applications in various industries, serving different purposes such as catalysts, electronics, drug carriers, magnetic and optical materials, pigments, and sensors. Exploring innovative procedures for NP synthesis is crucial to control properties like composition, crystallinity, morphology, and size distribution [96]. Materials comprised of NPs exhibit distinct optical properties, encompassing high or low refractive indices, remarkable transparency, novel photoluminescence characteristics and PC features [97].

The optical properties of a material, such as its refractive index and absorption coefficient, play a crucial role in determining its performance in a filter within a TPV system. In the context of PCs, the porosity, representing the void fraction or open space in the material, is a key factor. Porosity influences the effective refractive index and, consequently, the photonic bandgap properties, directly affecting the material's filtering capability in a TPV system [98], [99]. It is essential to note that the pore size must be significantly smaller than the wavelength of light. Additionally, to

prevent scattering, the distribution of pores needs to be homogeneous. Lorentz–Lorenz Equation (Eq. 1 and Eq. 2) was used to determine the  $n$  and  $\kappa$  values of this nanoporous film [100].

$$P = 1 - \frac{n^2 - 1}{n_d^2 - 1} \quad (1)$$

$$P = 1 - \frac{\kappa^2 - 1}{\kappa_d^2 - 1} \quad (2)$$

Where  $n$  is the refractive index of the porous film and  $n_d$  is the refractive index of the nonporous film. Similarly,  $\kappa$  is the imaginary refractive index of the porous film and  $\kappa_d$  is the refractive index of the nonporous film. Also,  $P$  is the porosity.

### 2.3.1 Preparation of Nanoparticle Films for Optical Application

There are different methods to create a film of NPs with a uniform structure, such as aerosol spray methods and NP dispersing methods. Aerosol spray methods, like spray pyrolysis, spray drying, and flame spray methods, are straightforward and quick for processing. They can be employed to prepare transparent conductive NPs, composite particles, and porous particles [96].

Creating size-controllable sub-micrometer particles with organized pores using spray drying is of interest, especially when using metal oxide NPs. It is possible to make porous particles from various oxide materials, provided colloidal oxide NPs are available. One important condition is that the dispersing medium of the colloid matches that of the organic beads to prevent unexpected reactions or agglomerations during mixing. The precursor for this method involves a mixture of two colloids—one with silica NPs of various sizes and the other with polymer (polystyrene latex) beads ranging from 10 nm to 100 nm [101].

The development of techniques for dispersing NPs into a solvent or monomer is crucial. Various mechanical processing methods, like agitator disks, colloid mills, high-pressure homogenizers,

triple roller mills, ball mills, and sand mills, have been developed to disperse agglomerated particles in liquids.

### **2.3.2 Coating Techniques for Making Nanoparticle Films**

Materials with 1D, 2D, or 3D structures have grabbed attention for their potential in optical applications. NPs, in particular, can play a role in optical materials. There are different ways to coat NPs to make PCs. Two common techniques for coating porous films evenly are dip-coating and spin-coating:

Dip-coating is used to produce 3D ordered pores in silica films, ranging from 40 to 1000 nm in size. This method involves dipping a sample in a solution, where a self-assembled organic (polystyrene) colloidal template is filled with silica NPs. Precursors with a mixed colloid of silica NPs and polystyrene particles are applied to coat a silicon wafer or glass substrate [102], [103].

Spin coating is a suitable method for creating uniform films on flat materials. It has advantages like a relatively short manufacturing time, cost-effectiveness, and the ability to cover large surfaces. Additionally, high spinning speeds enable the adsorption, rearrangement, and elimination of weakly bonded materials in a short processing time [104], [105].

## **2.4 Fabrication and Characterization of Graded Index One-Dimensional Photonic Crystal Thin Films**

This section details the techniques employed for the fabrication and characterization of 1DPC thin films with a graded-index structure.

Recent literature reports various emerging methods for fabricating graded-index films, such as lithography, wet etching, integrated nano-island coating arrays on nano-conical-frustum arrays, improved metal-induced chemical etching, oblique-angle deposition, electron beam evaporation, ion beam-assisted deposition, plasma-enhanced chemical vapor deposition, and the sol-gel process [39], [106]–[110]. For instance, Gaëtan and colleagues fabricated a nanoporous SiO<sub>2</sub>-based film with a low refractive index for large-surface anti-reflection coating applications [111]. Different techniques, including controlling the thermal annealing time process of ZrO<sub>2</sub> layer [112], were used to make graded index ZrO<sub>2</sub>. In another study, a six-layer graded-refractive index antireflection coating made of indium tin oxide (ITO) was created on GaInN LEDs to replace the common dense ITO coating [113]. This coating, fabricated by oblique-angle deposition, showed enhanced light-extraction efficiency due to reduced Fresnel reflection at the semiconductor–air interface. In such a coating, each layer has a refractive index individually tuned to form a stack with the refractive index graded from its dense materials value down to the value close to that of air for optimal anti-reflection performance [114].

Oblique-angle deposition is a vapor deposition technique often used to make thin films with a nanostructure, predesigned tilt angle, and controllable porosity. The precise control of porosity allows for controlling refractive indices ranging from  $n_L=1.09$  to  $n_H=2.6$ . As a result, almost all graded index profiles can be achieved using this technique [113]. As an example, in Figure 10 shows SEM images of a TiO<sub>2</sub>/SiO<sub>2</sub> 1DPC with graded index of refraction achieved with this method [114]. In Figure 11, the total reflectance of a graded-index sample at different wavelengths (633 nm, 830 nm, and 904 nm) for TE-polarized light. Additionally, there's a comparison with a quarter-wave coating. Overall, the reflectance is minimized for graded-index stack structure compared to quarter-wave stack for all angles of incident [114].

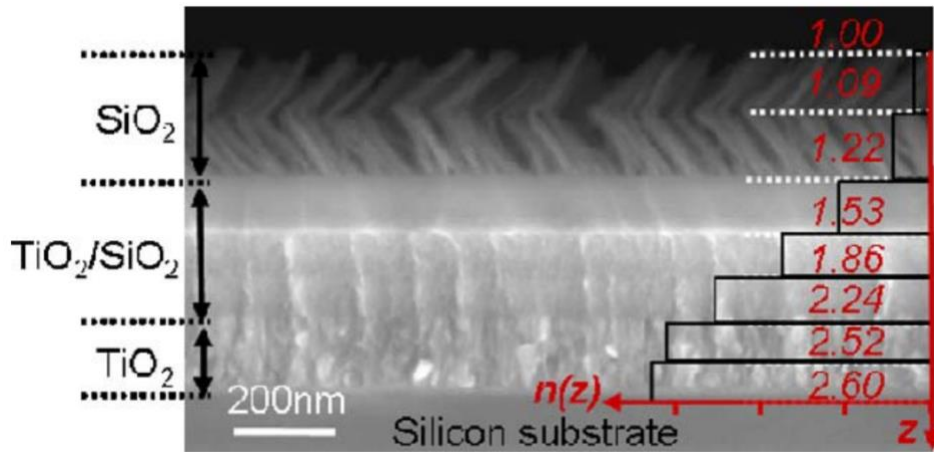


Figure 10. SEM images of a TiO<sub>2</sub>/SiO<sub>2</sub> 1DPC with graded index of refraction (Reprinted with permission from Ref. [115], The Optical Society)

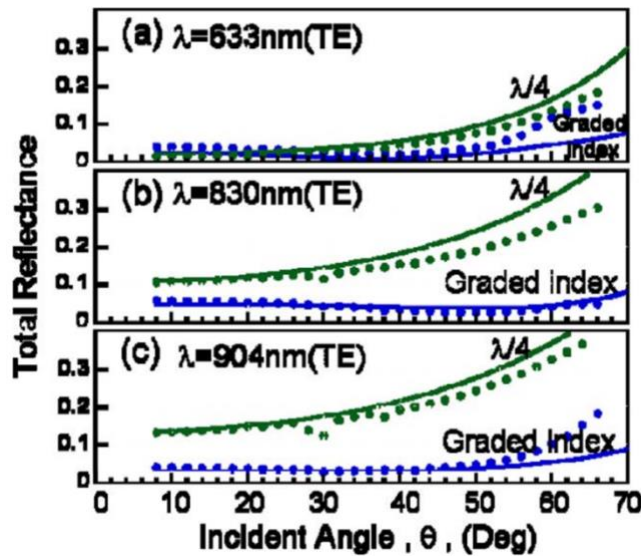


Figure 11. total reflectance at  $\lambda=633\text{ nm}$ ,  $830\text{ nm}$ , and  $904\text{ nm}$  for both quarter-wave and graded-index AR-coating samples (Reprinted with permission from Ref. [115], The Optical Society).

## 2.5 Energy Balance in Thermophotovoltaic Components

To ensure the conservation of total energy in a TPV system, it is imperative that the energy entering the system equals the energy exiting it. When examining a component, like an optical filter, the

energy balance is expressed as follows: incoming energy (incident) must be equivalent to the sum of absorbed, reflected, and transmitted energy (energy out). This relationship is mathematically defined as:

$$a(\lambda) + t(\lambda) + r(\lambda) = 1 \quad (3)$$

Here  $a$ ,  $t$ , and  $r$  represent absorbance, transmittance, and reflectance, respectively. These parameters are functions of wavelength ( $\lambda$ ), incident angle ( $\theta$ ), and the optical properties of the material, such as refractive index ( $n$ ) and extinction coefficient ( $\kappa$ ).

According to Kirchhoff's law of thermal radiation, the emissivity ( $\varepsilon$ ) of an object is equal to its absorptivity ( $a$ ) for a given wavelength:

$$\varepsilon(\lambda) = a(\lambda) \quad (4)$$

Here  $\varepsilon$  denotes emittance.

Where all these parameters are functions of wavelength, incident angle and the material's optical properties such as refractive index ( $n$ ) and extinction coefficient ( $\kappa$ ).

An opaque surface has no transmittance ( $T(\lambda) = 0$ ). When an opaque surface reflects no radiation, it acts as a perfect absorber, absorbing all incident radiation. This type of surface is commonly referred to as a black surface or a BB. In the simulation performed in this thesis, the emitter is assumed to behave like a BB. Consequently, all the radiation directed toward the emitter is considered as absorbed or recycled by the emitter. Figure 12 illustrates BB radiation at various temperatures. As per Planck's law, an increase in emitter temperature leads to a shift in radiation towards a lower wavelength region. This shift results in more radiated energy falling into the in-band region. Therefore, recycling out-of-band photons has a dual advantage: it reduces out-of-

band loss in the system and concurrently recycles this energy to elevate the emitter temperature. This energy balance leads to a significant finding in optimizing the design of an optical filter. Maximizing out-of-band without affecting the transmittance of in-band radiation is crucial for creating a filter that effectively mirrors the unusable photons.

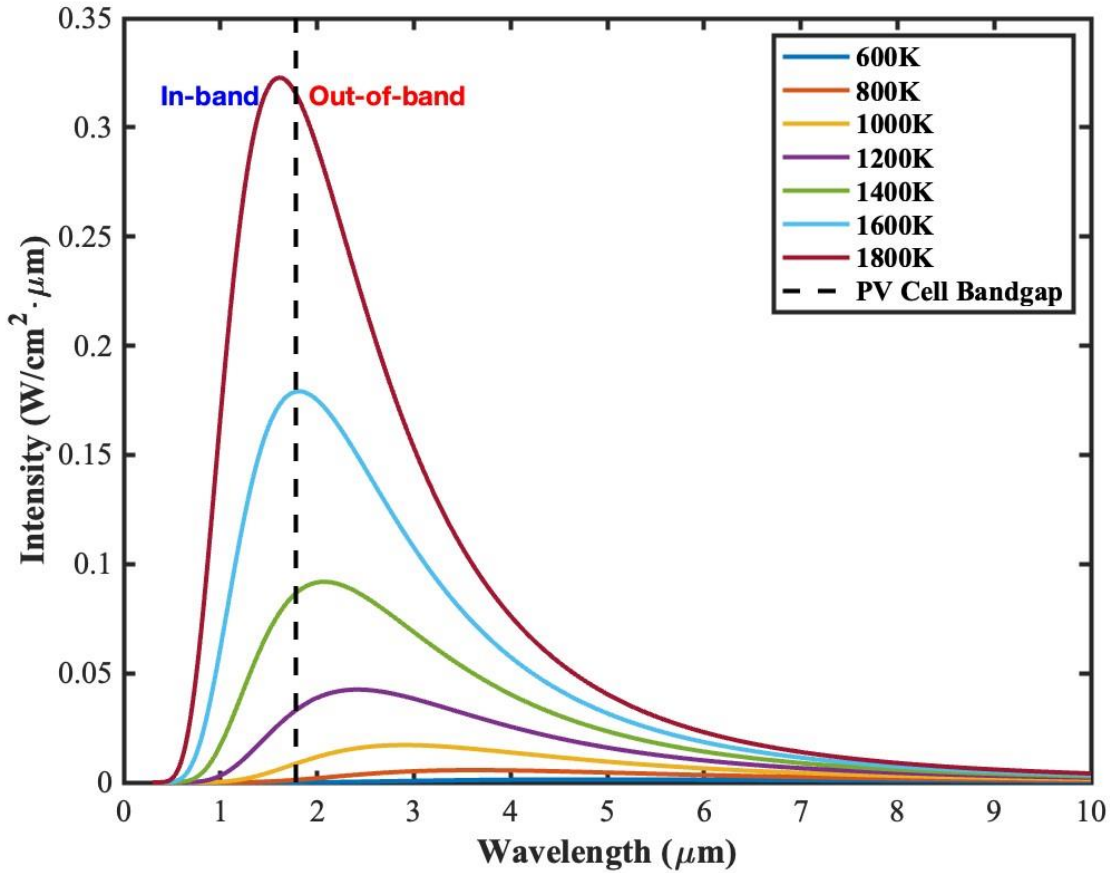


Figure 12. BB radiation spectra at different temperatures.

In summary, this background chapter establishes a foundation that intertwines the principles of PCs, TPV systems, and optical properties of nanoparticles. This synthesis is vital for the subsequent exploration and optimization of TPV systems using 1DPC as an optical filter.



### **3 Methodology**

The last chapter provides a detailed examination of the TPV system, including its components, spectral control, and a literature review of optical filters, specifically focusing on 1DPCs. It delves into discussions on BB emitters and GaSb PV cells. Additionally, a brief overview of the optical properties and preparation methods of NPs, a material crucial to this thesis, was included. This chapter breaks down the simulation process into three clear subsections to fulfill the first objective. Firstly, the TPV system and the 1DPC optical filters modeled in this work are described. Six different 1DPC filters with structural variations like quarter-wave, modified quarter-wave, and graded indices stacks are analyzed, examining their impact on TPV systems. The optical properties of SiO<sub>2</sub> NP and ZrO<sub>2</sub> films are also covered. In the second subsection of this chapter, a detailed methodology for calculating the efficiency and electrical power output of TPV systems is provided. In the third subsection, it is explained how this numerical study incorporates the Wave Optics Module in COMSOL Multiphysics, using the FEM to analyze electromagnetic wave behavior in optical structures.

#### **3.1 Description of TPV Systems and 1DPC optical filters**

The TPV system modelled in this work consists of a planar emitter and PV cell. The emitter is assumed to be a BB. The PV cell is a GaSb cell with an electronic bandgap energy of  $E_g = 0.73$  eV, which corresponds to a cut-off wavelength of  $1.78 \mu\text{m}$ . A 1DPC, functioning as a selective filter, is placed between the emitter and the GaSb cell. In this study, the effects of six different

1DPC filters consisting of five bi-layers of 30% porous SiO<sub>2</sub> NP films and solid ZrO<sub>2</sub> are films on the performance of the ideal TPV system shown in Figure. 13 a.

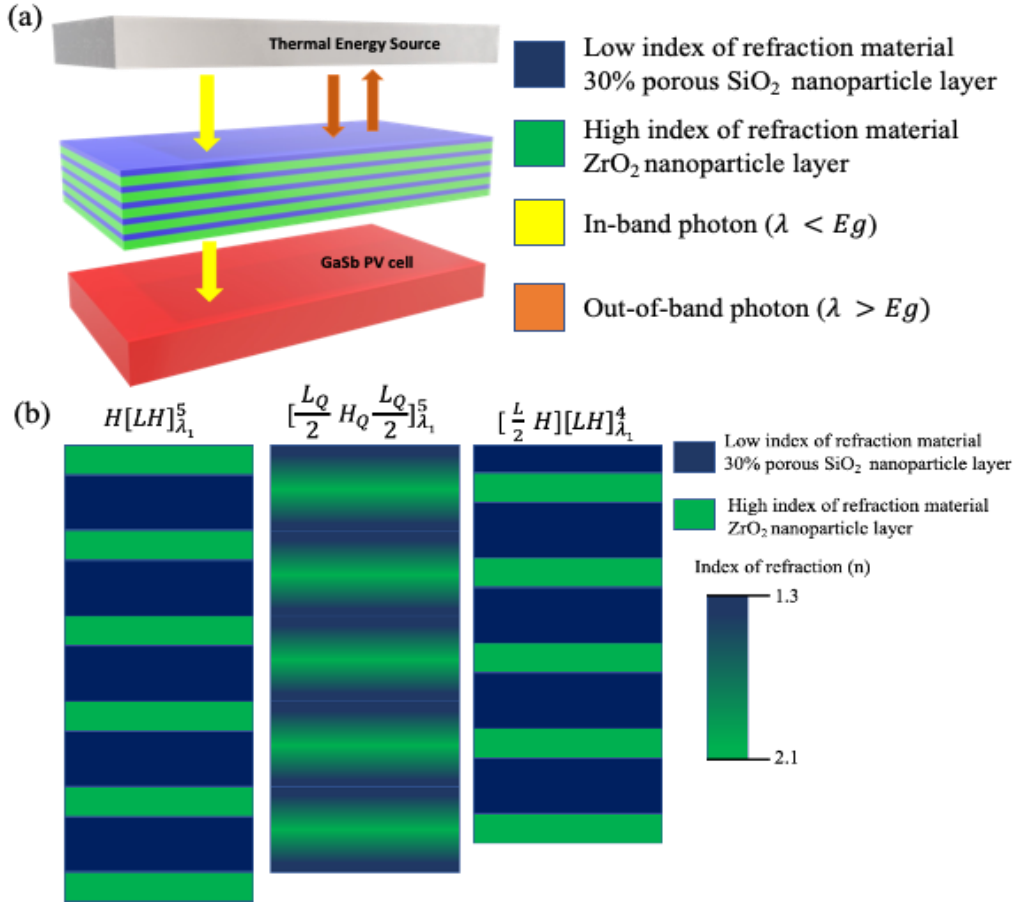


Figure 13. Spectral control in a TPV system with a front side optical filter. (b) Schematic diagram of a 1D PC in the form of a quarter-wave stack ( $H[LH]_{\lambda_1}^5$ ), a 1DPC filter with graded indices of refraction at its internal interfaces ( $[\frac{L_Q}{2} H_Q \frac{L_Q}{2}]_{\lambda_1}^5$ ) and a quarter-wave stack wherein the thickness of its top layer is reduced to half the thickness of the other layers within the stack ( $[\frac{L}{2} H][LH]_{\lambda_1}^4$ ).

Table 1. Notation, structure, and peak position of the six TPV filters

Filter No.	Notation	Structure	Peak position (s) ( $\mu\text{m}$ )
1	$H[LH]_{\lambda_1}^5$	Quarter wave, single	2.4

2	$[\frac{L_Q}{2} H_Q \frac{L_Q}{2}]_{\lambda_1}^5$	Quintic stack, single	2.2
3	$[\frac{L}{2} H][LH]_{\lambda_1}^4$	Modified quarter-wave stack, single	2.4
4	$H[LH]_{\lambda_1}^5 [LH]_{\lambda_2}^5$	Quarter-wave stack, double	2.4, 3.6
5	$[\frac{L_Q}{2} H_Q \frac{L_Q}{2}]_{\lambda_1}^5 [\frac{L_Q}{2} H_Q \frac{L_Q}{2}]_{\lambda_2}^5$	Quintic stack, double	2.2, 3.4
6	$[\frac{L}{2} H][LH]_{\lambda_1}^4 [LH]_{\lambda_2}^5$	Modified quarter-wave stack, double	2.4, 3.6

Figure. 14 illustrates the spectral reflectance at normal incidence for  $H[LH]_{\lambda_0}^P$  multilayered structures, where the number of periods,  $P$ , varies from 2 to 5. Generally, an increase in  $P$  results in higher spectral reflectance. Specifically, the reflectance peak within the photonic stop-band region significantly rises with increasing  $P$ , reaching >99% for  $P=5$ . However, as  $P$  increases, the width of these reflection peaks becomes narrower. Additionally,  $H[LH]_{\lambda_0}^P$  structures display noticeable reflection ripples in the passband region due to variations in their refractive index profile. In the context of a TPV system, these reflectance peaks in the passband region led to a reduction in the radiant power reaching the GaSb PV cell.

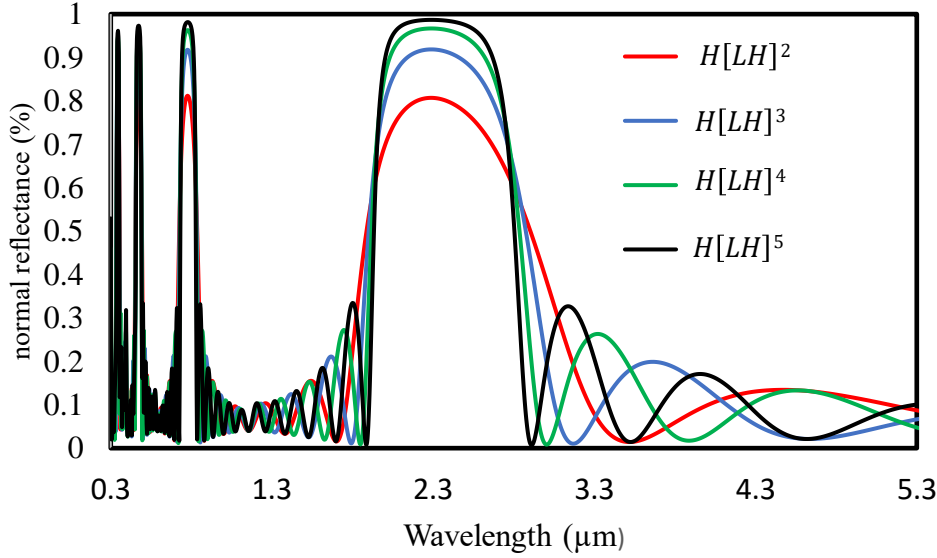


Figure 14. Normal reflectance for 1DPC with  $H[LH]^2$ ,  $H[LH]^3$ ,  $H[LH]^4$  and  $H[LH]^5$  arrangements.

The notations used to denote the six different 1DPC filters are listed in Table 1. The first 1DPC, as shown in Figure 13 b, is a quarter-wave stack comprised of SiO<sub>2</sub> NPs and is denoted as  $H[LH]_{\lambda_1}^5$ . In this notation H and L refer to layers of the high and low index materials, respectively. The superscript refers to the number of times the layers within the brackets are repeated (e.g. the first 1DPC is a quarter-wave stack comprised of five and a half bilayers; the uppermost layer is made from the high index of refraction layer and there are five repeating bilayers comprised of alternating layers of low and high indices of refraction beneath this). The subscript indicates the peak reflectance position, in units of  $\mu\text{m}$ , for the stack comprised of the alternating layers within the brackets. For example, for the first 1DPC the 2.4 indicates that the peak reflectance position of the stack of layers denoted as  $H[LH]_{2.4}^5$  is 2.4  $\mu\text{m}$ . The interfaces within the second 1DPC filter listed in Table 1, which is denoted as  $[\frac{LQ}{2} H_Q \frac{LQ}{2}]_{2.2}^5$ , have a graded index of refraction with a

profile shown by the blue line in Figure 14, b. The “Q” in the notation indicates the interfacial layers within the stack are graded with a profile that can be described with a quintic function. Furthermore, when H or L is divided by 2 it indicates the thickness of the layer is reduced to half its value. For example, the notation  $[\frac{L_Q}{2} H_Q \frac{L_Q}{2}]_{2.2}^5$  indicates the thicknesses of the low index of refraction layers are one-eighth of the peak position wavelength (in the repeated layers the two adjacent  $\frac{L_Q}{2}$  layers form one quarter-wave layer, as all 1DPCs considered in this work are in the form of a quarter-wave stack). The third 1DPC filter is similar to the first, but the thickness of the top layer has been modified by reducing its thickness to half of its original thickness, which increases the transmittance of in-band photons, although with the trade-off of reducing the reflectance of the out-of-band photons. The fourth to sixth filters are each composed of two 1DPCs with different peak positions that are stacked on top of each other. Their internal structures are similar to those of the initial three filters: a quarter-wave stack, a graded index, and a modified quarter-wave stack. The reflectance peak positions for the 1DPCs for the six cases are given in the last column in Table 1 and for Cases 4, 5, and 6 two values are given to indicate the peak positions of the two 1DPCs stacked on top of each other. As described further in Section 4. 2, the reflectance peak positions are determined by optimizing the efficiency of the TPV system and the resulting electrical output power when the emitter is at a temperature of 1800 K.

The real and imaginary components of the index of refraction of SiO<sub>2</sub> and ZrO<sub>2</sub> were taken into consideration. The optical properties of SiO<sub>2</sub> and ZrO<sub>2</sub> provided by Jiang et. al. [116] and Yusoh et. al. [117], [118], respectively, were used in the simulation. The n and k spectra used to perform the simulations are shown in Figure (11, a).

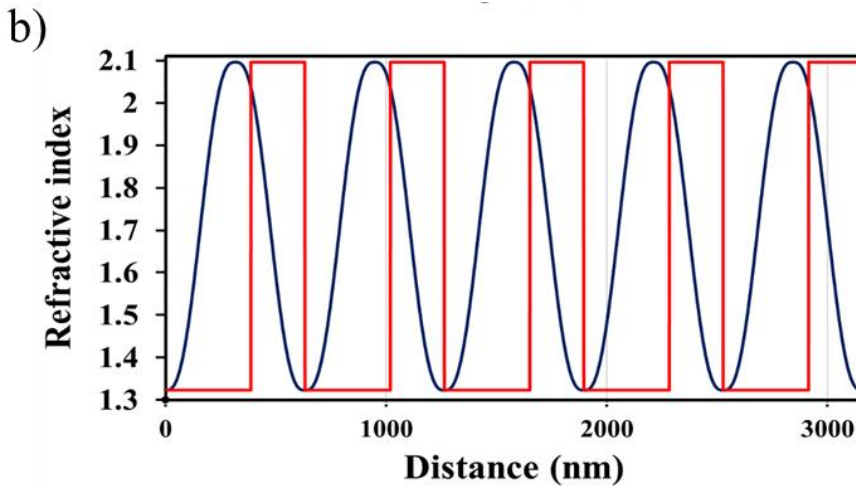
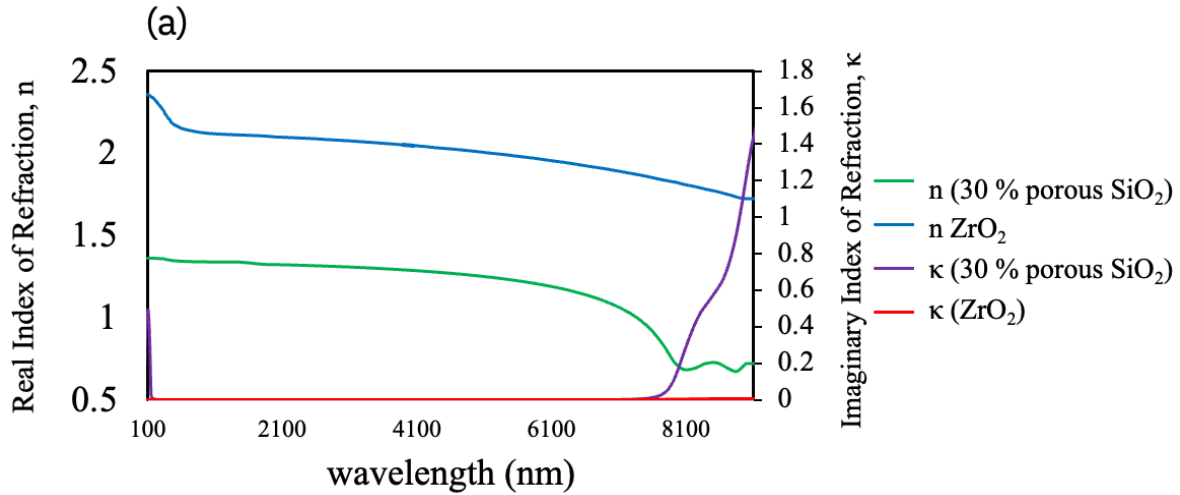


Figure 15. (a) Refractive index ( $n$ ) and extinction coefficient ( $\kappa$ ) spectra of  $\text{ZrO}_2$  and 30% porous  $\text{SiO}_2$ . (b) Refractive index profile for  $[\text{LH}]_{\lambda_1}^5$  and  $[\frac{\text{LQ}}{2} \text{H}_Q \frac{\text{LQ}}{2}]_{\lambda_1}^5$  filters.

The optical properties of  $\text{SiO}_2$  were adjusted to account for the fact that the  $\text{SiO}_2$  NP films are porous. The methodology to modify  $n$  and  $\kappa$  is provided in Section 2. 3. The porosity of the  $\text{SiO}_2$  NP films are assumed to be 30%. Furthermore, the refractive indices of the materials are wavelength dependent.

If the  $\text{SiO}_2$  spheres are in a close-packing arrangement, it is proved that the highest average density or in other words, fraction of space occupied by spheres that can be achieved by a lattice packing

is 0.745 [119]. This is porosity of 26.5 %. which in this simulation, it is assumed to have 30 % porosity for SiO<sub>2</sub>.

### 3.2 Methods for Determining Filter Reflectance, Transmittance, and Absorptance

The Wave Optics Module of COMSOL Multiphysics was used to determine the reflectance, transmittance, and absorptance spectra of the six optical filters described in Section 3-1. The thickness of each layer within the 1DPCs is determined using Eq. 5 and Eq. 6. In these equations,  $n$  is an index of refraction and  $\lambda_c$  is the wavelength at the centre of the photonic bandgap. The reflectance peak centre wavelength,  $\lambda_c$ , is set to the value that optimizes TPV system efficiency.

$$d_L = \frac{\lambda_c}{4 \times n_L} \quad (5)$$

$$d_H = \frac{\lambda_c}{4 \times n_H} \quad (6)$$

Table 2. Peak position, low and high refractive index layer thickness.

Peak position ( $\mu\text{m}$ )	$d_L$ (nm)	$d_H$ (nm)	$d_{H+L}$ (nm)
2.2	415	262	678
2.4	453	286	739
3.4	642	405	1048
3.6	680	429	1109

For filters 2 and 5 the graded refractive index profiles at their internal interfaces are defined using the quintic functions given as Eq. 7 and Eq. 8. Eq. 7 describes gradual change from a minimum index ( $n_L$ ) to maximum index ( $n_H$ ) and Eq. 8 describes gradual change from a maximum index ( $n_H$ ) to minimum index ( $n_L$ ).

In equation 7, 20 points in equal interval are selected from this function to form a gradual increase and decrease in the refractive index profile of the filters. Thus, a bilayer within the 1DPC is discretized into 40 sub-layers or thin slices as shown in Figure 16.

$$n = n_L + (n_H - n_L) (10d^3 - 15d^4 + 6d^5), 0 \leq d \leq 1 \quad (7)$$

$$n = n_H + (n_L - n_H) (10 \times (1-d)^3 - 15 \times (1-d)^4 + 6 \times (1-d)^5), 0 \leq d \leq 1 \quad (8)$$

Figure 16 shows the index of refraction profile for bilayers within the  $[\frac{L}{2} H \frac{L}{2}]_{\lambda_1}^1$  and  $[\frac{L_Q}{2} H_Q \frac{L_Q}{2}]_{\lambda_1}^1$  structures. The index of refraction gradually increases in 20 sub-layer steps from the lowest value (which is 1.323 when  $\lambda = 1780$  nm) to the highest value (which is 2.096 when  $\lambda = 1780$  nm), and then gradually decreases back to the lowest value in 20 sub-layer steps.

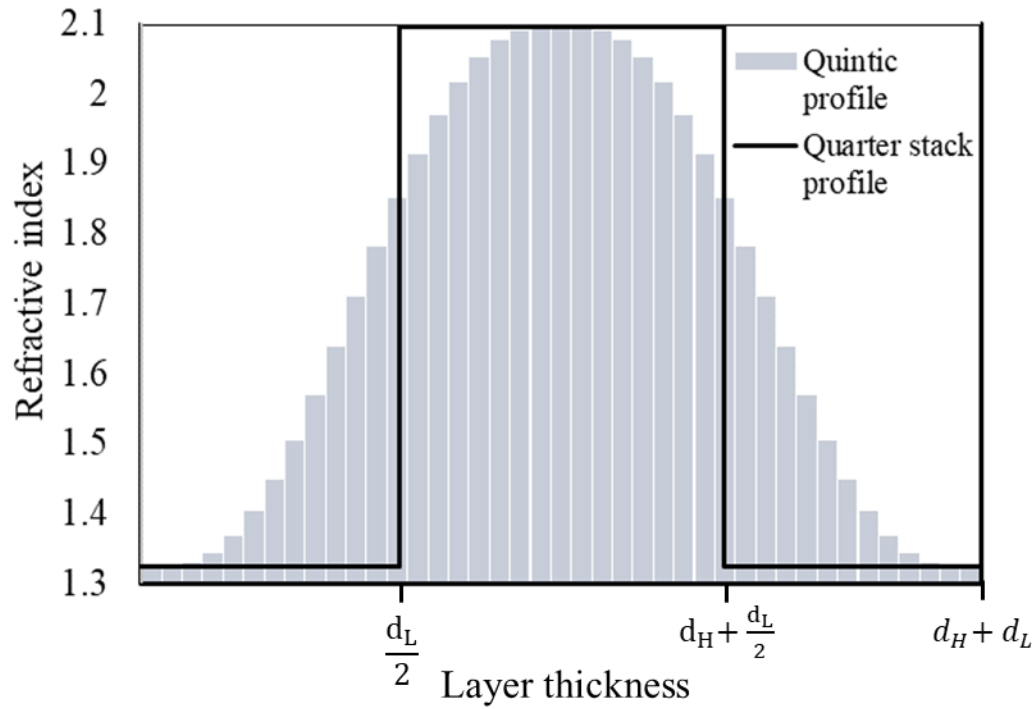


Figure 16. Quintic and quarter wave stack profiles.

The total thickness of the  $[\frac{L_Q}{2} H_Q \frac{L_Q}{2}]_{\lambda_1}^P$  layer ( $d_{H+L}$ ) is equal to the thickness of corresponding quarter-wave stack ( $[LH]_{\lambda_1}^P$ ) ( $d_{H+L} = d_H + d_L$ ) (Figure 16). The thicknesses of the sub-layers within a given stack are equal and are determined by dividing  $d_{H+L}$  by the number of sub-layers.

The transmittance, reflectance, and absorptance are calculated for both TE and TM polarizations as the angle of incidence varies in increments of  $10^\circ$  from the direction normal to the planes of the PC (e.g., from  $0^\circ$  to  $90^\circ$  in  $10^\circ$  steps). As an illustration of this process, the reflectance spectrum of TM and TE polarizations at  $0^\circ$ ,  $20^\circ$ ,  $40^\circ$ , and  $60^\circ$  angles for a 1DPC  $ZrO_2/SiO_2$  NPs filter with a  $[\frac{L}{2} H][LH]_{2.3}^4[LH]_{3.4}^5$  arrangement is presented in Figure 17, (a) and (b). The average of the TM and TE polarized modes is considered in calculating the reflectance, transmittance, and absorptance spectra of the filter.

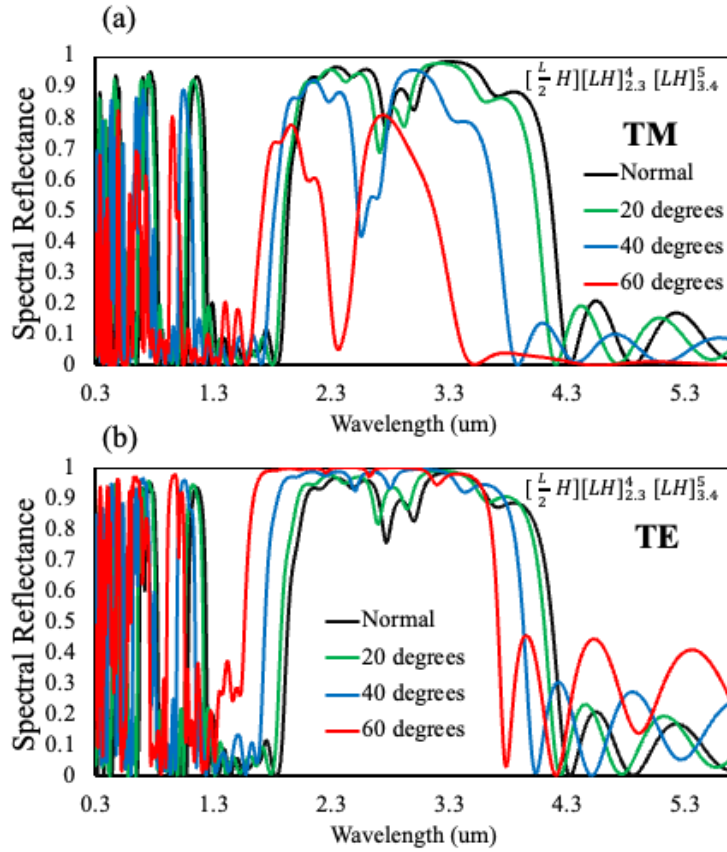


Figure 17. (a) TM and (b) TE polarization of 1D  $ZrO_2/SiO_2$  PC in form of  $[\frac{L}{2} H][LH]_{2.3}^4 [LH]_{3.4}^5$  at different incident angles.

Wave optics analysis is done in the wavelength region from 0.3 to 10  $\mu\text{m}$  (4.133 eV to 0.124 eV), in increments of 2 nm between 0.3 and 3  $\mu\text{m}$  (4.133 eV to 0.413 eV) and increments of 10 nm between 3 and 10  $\mu\text{m}$  (0.413 eV to 0.124 eV). It is assumed the materials above and below the filters are air and glass, respectively. Glass is assumed to be semi-infinite with a refractive index of 1.4. It is assumed that all light propagating through the glass is incident onto the GaSb PV cell, such that the effects of the rear side of the glass substrate are neglected.

In this work the focus is to reduce inband reflection due to presence of frontside optical filter and this work is not aiming to reduce reflection due to PV cell itself. However, the index of refraction for glass substrate has negligible effect on the results, a sensitivity analysis is performed to show

reflectance of the same filter (in this case  $\frac{L}{2}H[LH]^{4}_{2.3}$ ) with different index of refraction for the glass substrate (Figure 18).

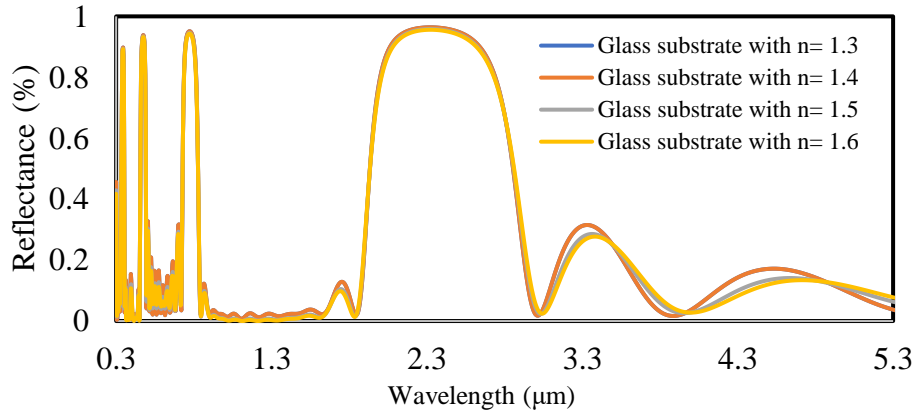


Figure 18. Reflectance of  $\frac{L}{2}H[LH]^{4}_{2.3}$  with different index of refraction for glass substrate.

The transmittance, reflectance and absorptance spectra are used to determine the power output and efficiency of the TPV systems using the analytical methods explained in Section 2.3, which are carried out using MATLAB. It is also important to note that the PV cell is assumed to be held at a constant temperature of 298 K, equal to the temperature of the surrounding environment. The amount of electric power generated is determined using the radiation spectrum incident onto the PV cell and the External Quantum Efficiency (EQE) of the GaSb PV cell [120].

### 3.3 Calculating TPV System Efficiency and Electrical Power Output

The reflectance, transmittance and absorptance spectra of the optical filters determined in Section 3.2 are used to calculate the TPV system efficiency and power output. MATLAB software is used

to carry out the calculations for the TPV configuration shown in Figure 6 b and it is assumed the emitter, filter, and PV cell extend to infinity in the planar directions.

The Stefan–Boltzmann law is used to calculate the radiative heat transfer from the emitter surface (Eq. 9). The emitter is assumed to be a BB at a constant uniform temperature and Equation 10 can be used to calculate the emitted power.

$$P_{\text{emission}} = \int_0^{\infty} \varepsilon_{\text{emt}}(\lambda) \cdot E_{\lambda}(\lambda, T) \cdot d\lambda \quad (9)$$

$$P_{\text{emission}} = \sigma \cdot T^4 \quad (10)$$

Where  $\varepsilon_{\text{emt}}(\lambda)$  is the emissivity, T is the temperature of the emitter, and  $E_{\lambda}(\lambda, T)$  is the spectral emissive power from the emitter. The radiation spectrum for the emitter is calculated using Planck's law (Eq. 11). In this equation  $E_{b\lambda}(\lambda, T)$  is the spectral emissive power from a BB at temperature T.

$$E_{b\lambda}(\lambda, T) = \frac{2\pi hc^2}{\lambda^5 \left[ \exp\left(\frac{hc}{\lambda k_0 T}\right) - 1 \right]} \quad (11)$$

To evaluate the performance of the optical filters described in Section 3.1, and to facilitate their comparison with other types of filters reported in the literature, herein we define optical parameters: the fraction of in-band emission power that is transmitted through the filter ( $\bar{T}_{in-band}^P$ ), the fraction of out-of-band emission power that is reflected by the filter ( $\bar{R}_{out-of-band}^P$ ), and the fraction of in-band ( $\bar{A}_{in-band}^P$ ) and out-of-band ( $\bar{A}_{out-of-band}^P$ ) emission power that are absorbed by the filter, are determined using Equations 12, 13, 14 and 15, respectively.

$$\bar{T}_{\text{in-band}}^P = \frac{\int_0^{\lambda_g} \int_0^{2\pi} \int_0^{\frac{\pi}{2}} \bar{T}_\lambda(\lambda, \theta) \cdot E_{b\lambda}(\lambda, T) \cdot \cos\theta \sin\theta \cdot d\theta \cdot d\varphi \cdot d\lambda}{\int_0^{\lambda_g} \int_0^{2\pi} \int_0^{\frac{\pi}{2}} E_{b\lambda}(\lambda, T) \cdot \cos\theta \sin\theta \cdot d\theta \cdot d\varphi \cdot d\lambda} \times 100 \quad (12)$$

$$\bar{R}_{\text{out-of-band}}^P = \frac{\int_{\lambda_g}^{\infty} \int_0^{2\pi} \int_0^{\frac{\pi}{2}} \bar{R}_\lambda(\lambda, \theta) \cdot E_{b\lambda}(\lambda, T) \cdot \cos\theta \sin\theta \cdot d\theta \cdot d\varphi \cdot d\lambda}{\int_{\lambda_g}^{\infty} \int_0^{2\pi} \int_0^{\frac{\pi}{2}} E_{b\lambda}(\lambda, T) \cdot \cos\theta \sin\theta \cdot d\theta \cdot d\varphi \cdot d\lambda} \times 100 \quad (13)$$

$$\bar{A}_{\text{in-band}}^P = \frac{\int_0^{\lambda_g} \int_0^{2\pi} \int_0^{\frac{\pi}{2}} \bar{A}_\lambda(\lambda, \theta) \cdot E_{b\lambda}(\lambda, T) \cdot \cos\theta \sin\theta \cdot d\theta \cdot d\varphi \cdot d\lambda}{\int_0^{\lambda_g} \int_0^{2\pi} \int_0^{\frac{\pi}{2}} E_{b\lambda}(\lambda, T) \cdot \cos\theta \sin\theta \cdot d\theta \cdot d\varphi \cdot d\lambda} \times 100 \quad (14)$$

$$\bar{A}_{\text{out-of-band}}^P = \frac{\int_{\lambda_g}^{\infty} \int_0^{2\pi} \int_0^{\frac{\pi}{2}} \bar{A}_\lambda(\lambda, \theta) \cdot E_{b\lambda}(\lambda, T) \cdot \cos\theta \sin\theta \cdot d\theta \cdot d\varphi \cdot d\lambda}{\int_{\lambda_g}^{\infty} \int_0^{2\pi} \int_0^{\frac{\pi}{2}} E_{b\lambda}(\lambda, T) \cdot \cos\theta \sin\theta \cdot d\theta \cdot d\varphi \cdot d\lambda} \times 100 \quad (15)$$

It is desirable for the filter in TPV systems to exhibit high values of  $\bar{T}_{\text{in-band}}^P$  and  $\bar{R}_{\text{out-of-band}}^P$  and a low values of  $\bar{A}_{\text{in-band}}^P$  and  $\bar{A}_{\text{out-of-band}}^P$ . Increasing the amount of in-band radiant power that is transmitted increases the generated output power of the TPV system, while increasing the reflectance of the out-of-band radiative power increases the amount of radiant energy reflected back to the emitter (e.g. the number of recycled photons), which increases the temperature of the emitter which in turn increases the system efficiency.

The efficiency of the TPV system is given by Equation 16:

$$\eta_{\text{TPV}} = \frac{P_{\text{PV-out}}}{P_{\text{input}}} \times 100\% \quad (16)$$

Where  $P_{\text{PV-out}}$  is the output electric power from the PV cell.  $P_{\text{input}}$  is the power supplied to the emitter to maintain its temperature at a constant set value.  $P_{\text{input}}$  is equal to the BB emissive power minus what is reflected by the filter and is given by Equation. 17.

$$P_{\text{input}} = \int_0^{\infty} \int_0^{2\pi} \int_0^{\frac{\pi}{2}} E_b(\lambda, T_{\text{Emmitter}}) \cdot \bar{T}_{\text{BB} \rightarrow \text{PV}}(\lambda, \theta) \cdot \cos\theta \sin\theta \cdot d\theta \cdot d\varphi \cdot d\lambda -$$

$$\int_0^{\infty} \int_0^{2\pi} \int_0^{\frac{\pi}{2}} E_b(\lambda, T_{\text{PV}}) \cdot \bar{T}_{\text{PV} \rightarrow \text{BB}}(\lambda, \theta) \cdot \cos\theta \sin\theta \cdot d\theta \cdot d\varphi \cdot d\lambda \quad (17)$$

The electric power output from the PV cell is determined using Equations 18 to 22 [121]:

$$P_{\text{PV-out}} = V_{\text{OC}} \times J_{\text{SC}} \times \text{FF} \quad (18)$$

$$J_{\text{SC}} = F_{\text{PV}} \times q \times \int_0^{\lambda_g} \int_0^{2\pi} \int_0^{\frac{\pi}{2}} \frac{\lambda}{h \times c} \cdot E_{\lambda}(\lambda, T) \cdot T(\lambda, \theta)_{\text{BB} \rightarrow \text{PV}} \cdot \text{EQE}(\lambda) \cdot \cos\theta \sin\theta d\theta d\varphi d\lambda \quad (19)$$

$$V_{\text{OC}} = \frac{K_0 \times T_0}{q} \ln \left( \frac{J_{\text{SC}}}{J_s} + 1 \right) \quad (20)$$

$$J_s = (1.84 \times 10^{-3}) \times T_0^3 \times \exp \left( \frac{-E_g}{K_0 \times T_0} \right) \quad (\text{amps/cm}^2) \quad (21)$$

$$\text{FF} = \left( 1 - \frac{1}{\ln \left( \frac{J_{\text{SC}}}{J_s} \right)} \right) \times \left( 1 - \frac{\ln \left( \ln \left( \frac{J_{\text{SC}}}{J_s} \right) \right)}{\ln \left( \frac{J_{\text{SC}}}{J_s} \right)} \right) \quad (22)$$

Spectral efficiency ( $\eta_{\text{spec}}$ ) is calculated using Equation 23.

$$\eta_{\text{spec}}(T, \lambda_g) = \frac{\int_0^{\lambda_g} \int_0^{2\pi} \int_0^{\frac{\pi}{2}} E_b(\lambda, T) \cdot \bar{T}_{\text{BB} \rightarrow \text{PV}}(\lambda, \theta) \cdot \cos\theta \sin\theta \cdot d\theta \cdot d\varphi \cdot d\lambda}{\int_0^{\infty} \int_0^{2\pi} \int_0^{\frac{\pi}{2}} E_b(\lambda, T) \cdot \bar{T}_{\text{BB} \rightarrow \text{PV}}(\lambda, \theta) \cdot \cos\theta \sin\theta \cdot d\theta \cdot d\varphi \cdot d\lambda} \quad (23)$$

For in-band gray transmission and out-of-band gray reflection with a non-absorbing filter:

$$J_{\text{SC}} = F_{\text{PV}} \times q \times \bar{T}_{\text{in-band}}^{\text{P}} \times \int_0^{\lambda_g} \int_0^{2\pi} \int_0^{\frac{\pi}{2}} \frac{\lambda}{h \times c} \cdot E_{\lambda}(\lambda, T) \cdot \text{EQE}(\lambda) \cdot \cos\theta \sin\theta d\theta d\varphi d\lambda \quad (24)$$

$$P_{\text{input}} = \bar{T}_{\text{in-band}}^{\text{P}} \times \int_0^{\lambda_g} \int_0^{2\pi} \int_0^{\frac{\pi}{2}} E_b(\lambda, T_{\text{Emmitter}}) \cdot \cos\theta \sin\theta \cdot d\theta \cdot d\varphi \cdot d\lambda + \left[ 1 - \right.$$

$$\left. \bar{R}_{\text{out-of-band}}^{\text{P}} \right] \int_{\lambda_g}^{\infty} \int_0^{2\pi} \int_0^{\frac{\pi}{2}} E_b(\lambda, T_{\text{Emmitter}}) \cdot \cos\theta \sin\theta \cdot d\theta \cdot d\varphi \cdot d\lambda \quad (25)$$

$$\eta_{\text{spec}}(T, \lambda_g) = \frac{\bar{T}_{\text{in-band}}^P \times \int_0^{\lambda_g} \int_0^{2\pi} \int_0^{\frac{\pi}{2}} E_b(\lambda, T) \cdot \cos\theta \sin\theta \cdot d\theta \cdot d\phi \cdot d\lambda}{P_{\text{input}}} \quad (26)$$

Where  $V_{oc}$ ,  $J_{sc}$  and  $FF$  are the open-circuit voltage, short-circuit current density and fill factor for the PV cell, respectively. The other parameters in Equations 18 through 26 are: The emitter-to-PV cell view factor ( $F_{PV}$ ), the elementary charge ( $q$ ), Planck's constant ( $h$ ), the speed of light ( $c$ ), Boltzmann's constant ( $K_0$ ), the equilibrium temperature of the BB emitter ( $T$ ), the temperature of the PV cell ( $T_0$ ), the saturation current density ( $J_s$ ), and the energy bandgap of the PV cell ( $E_g$ ).  $T(\theta)_{BB \rightarrow PV}$  and  $R(\theta)_{BB \rightarrow BB}$  are the spectral transmittance and reflectance of the filter, respectively. In this work, the optical filter will transmit photons from the emitter towards the PV cell ( $T(\theta, \lambda)_{BB \rightarrow PV}$ ) or reflect emitted photons back to the emitter ( $R(\theta)_{BB \rightarrow BB}$ ) or absorbs corresponding photons.

Furthermore, it is assumed that all photons incident onto the PV cell are absorbed (its reflectance is zero) and  $EQE(\lambda)$  is the EQE of the GaSb PV cell. Also, it is assumed the TPV system is equipped with an adequate cooling system (shown in Figure 6 b) such that its temperature is constant at 298 K.

Moreover, the temperature of the BB herein is considered to vary from 1000 to 2000 K as emitters used in TPV systems are typically operated in this range. In addition, the selected wavelength spectrum (0.3 to 10  $\mu\text{m}$ ) covers 91% and 99% of the thermal radiation emitted from a BB at temperatures of 1000 K and 1800 K, respectively.

It can be noted that the methods described in this section can be used to evaluate the performance of optical filters if the fraction of in-band radiant power transmitted by the filter ( $T_{\text{in-band}}^P$ ) and the fraction of out-of-band radiant power reflected by the filter ( $R_{\text{out-of-band}}^P$ ) are known. While

$T(\lambda, \theta)_{BB \rightarrow PV}$  is a spectral and directional property of the filter,  $T_{in-band}^P$  and  $R_{out-of-band}^P$  are independent of direction and wavelength.

A parametric analysis (Figure 17) evaluating TPV efficiency as functions of  $T_{in-band}^P$  and  $R_{out-of-band}^P$  is presented in this study. Assuming a non-absorbing filter with wavelength-independent (gray) reflection and transmission in both in-band and out-of-band regions, an upper efficiency limit for TPV can be deduced. For in-band gray transmission and out-of-band gray reflection, Equations 23 to 26 can be used to determine the spectral and TPV system efficiency.

### **3.4 Wave Optics Module in COMSOL Multiphysics**

The Wave Optics Module in COMSOL Multiphysics is a powerful simulation tool that employs the FEM to analyze electromagnetic wave behavior in optical structures such as PC. With comprehensive 2D and 3D modeling capabilities, including Electromagnetic Waves, Frequency Domain (EWFd) with adaptive frequency sweeps and boundary mode analysis, it facilitates in-depth exploration of optical filter designs by considering various symmetries and dimensions, providing a versatile platform for optimizing optical component performance.

The Wave Optics Module has the capability to conduct simulations of high-frequency electromagnetic waves. In the context of this thesis, the focus lies on frequency domain simulations, eliminating the necessity for time-dependent simulations. This configuration aptly suits optical phenomena, components, and systems, encompassing materials characterized by both time-varying properties and frequency dispersion.

Within the Frequency Domain interface, the total electric field serves as the dependent variable. Given that the electric field exhibits spatial variations at the scale of a wavelength, it becomes imperative to ensure that the maximum mesh element size is a fraction of the wavelength. When this mesh requirement is met, the Frequency Domain interface proves highly adaptable for effectively tackling propagation and scattering problems.

Maxwell's equations, representing fundamental relationships among electromagnetic quantities, include:

Electric field intensity (E)

Electric displacement or electric flux density (D)

Magnetic field intensity (H)

Magnetic flux density (B)

Current density (J)

Electric charge density ( $\rho$ )

These equations can be expressed in either differential or integral form. The preference for the differential form arises because it leads to equations compatible with FEM. For general time-varying fields, Maxwell's equations take the form:

$$\nabla \times \mathbf{E} = - \partial \mathbf{B} / \partial t \quad (27)$$

$$\nabla \times \mathbf{H} = \mathbf{J} + \partial \mathbf{D} / \partial t \quad (28)$$

$$\nabla \cdot \mathbf{D} = \rho \quad (29)$$

$$\nabla \cdot \mathbf{B} = 0 \quad (30)$$

The first two equations, known as Maxwell-Ampère's law and Faraday's law, respectively, play crucial roles. Equations (29) and (30) represent the electric and magnetic forms of Gauss' law.

In Figure 19, the structure of 1DPCs for both quarter-wave and graded index structures are shown. In this study consists of a glass substrate with a refractive index of 1.4 ( $n_s=1.4$ ) and a thickness of 2000 nm, upon which layers of 1DPC are constructed. The uppermost layer is defined as air with a refractive index of 1 ( $n_a=1$ ).

Within the Electromagnetic Waves, Frequency Domain interface, Maxwell's equations are numerically solved for the specified geometry. For Transverse Electric (TE) mode, the electric field's component is solved for out-of-plane vector. Conversely, for Transverse Magnetic (TM) mode, the electric field's component is solved for in-plane vector.

Boundary conditions are specified as follows:

Port node is where electromagnetic energy enters or exits the structure, capable of launching and absorbing specific modes. Two ports are defined as periodic: Port 1, which is the entry point for electromagnetic energy with a set port excitation of 1 W, and Port 2, at which energy exits with no excitation. The electric field amplitude for TE mode is defined as (0, 0, 1) V/m across the x, y, and z directions. For TM mode, the magnetic field amplitude is prescribed as (0, 0, 1) A/m across the same directional components.

In the side walls shown by number 3, the floquet periodic boundary condition is applied along the +/- Y direction, and the Continuity periodic condition is employed in the +/- X direction. This

allows for the 1DPC to be conceptually extended to infinity along the +/- X direction by applying the same solution at source and boundaries.

Meshing: The maximum mesh element size in the COMSOL simulations throughout the filter region was 6 nm when the filter had a quarter-wave stack configuration (e.g. for Cases 1, 3, 4, and 6) and 1 nm when the interfaces within the filter had a graded index of refraction (Cases 2 and 5). This mesh size provides less than  $10^{-6}$  error with respect to 100 times finer maximum mesh element size for the cases wherein the 1DPCs have a graded index of refraction.

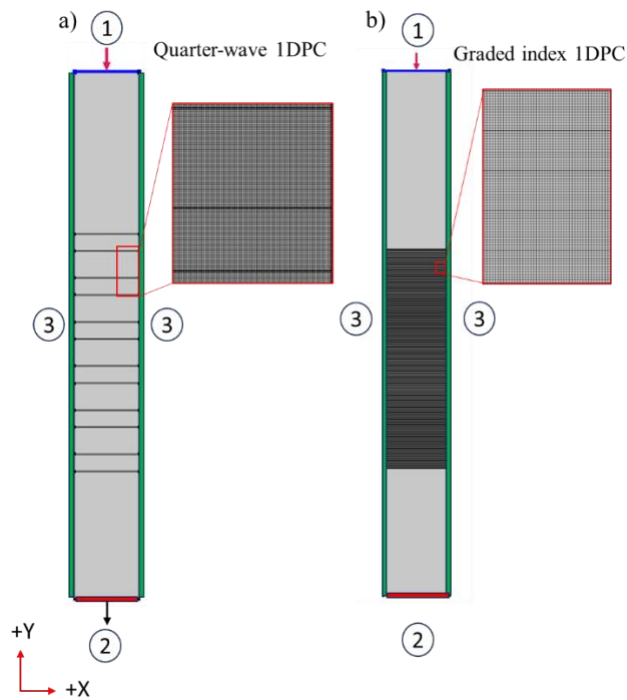


Figure 19. Quarter-wave and graded index 1DPC simulation in COMSOL interface

## 4 Results

The previous chapter thoroughly explained the methodology. This chapter discusses the numerical results in two main subsections. The first subsection evaluates the optical performance of single stack 1DPC filters, focusing on transmittance, reflectance, and absorption. This involves comparing the optical behavior of 1DPC filters with a graded index profile to traditional and modified quarter-wave stack arrangements.

To achieve the second objective, 1DPCs are designed as effective filters TPV systems. Enhancing photon recycling, a secondary 1DPC filter with a different peak wavelength is placed on top of the first. This stack increases out-of-band reflection. In-band transmittance, out-of-band reflectance, and in-band and out-of-band absorption are investigated for all six cases, taking into account various emitter temperatures.

The second subsection addresses the third objective: assessing TPV system efficiency and electrical power output for the six 1DPC filter. The peak wavelength position is optimized to provide the highest system efficiency.

### 4.1 Optical evaluation of designed filters

This section discusses the optical behaviour of the three primary form of 1DPC optical filters described in the previous chapter. The reflectance and transmittance spectra of single-stack filters at normal angle (Cases 1 to 3 in Table 1) are shown in Figure 20, a and 20, b.

The in-band transmittance for  $H[LH]_{2.4}^5$ , shown by the red line, has a fluctuating pattern that significantly reduces the useful energy received by the PV cell ( $\bar{T}_{in-band}^P$ ). In this quarter-wave

stack arrangement, the interaction of waves starts with the H index layer and then moves to the L index layer. This sudden change in index of refractrion reduce transmittanc within inband region. The  $[\frac{LQ}{2} H_Q \frac{LQ}{2}]_{2.2}^5$  filter, represented by the green line, exhibits increased in-band transmission but reduced out-of-band reflection. Waves interact with this graded index structure starting with the L index, and gradual increase in refractive index reduce the ripples in the transmission of electromagnetic waves. The results for the  $[\frac{L}{2} H][LH]_{2.4}^4$  filter are represented by the blue lines in Figure 20. The  $[\frac{L}{2} H][LH]_{2.4}^4$  filter is a modified quarter-wave stack structure where light enters the filter with an L index layer of reduced thickness. This modified structure provides high in-band transmission from 1  $\mu\text{m}$  to 1.8  $\mu\text{m}$  while maintaining higher out-of-band reflectance compared to filtes with a  $[\frac{LQ}{2} H_Q \frac{LQ}{2}]_{2.2}^5$  configuration. For all three cases, the peak positions have been selected to provide the highest TPV system efficiency. For  $[\frac{L}{2} H][LH]_{2.4}^4$  and  $H[LH]_{2.4}^5$  a reflectance peak wavelength of 2.4  $\mu\text{m}$  is selected , and for  $[\frac{LQ}{2} H_Q \frac{LQ}{2}]_{2.2}^5$  a reflectance peak wavelength of 2.2  $\mu\text{m}$  is selected. In general,  $[\frac{L}{2} H][LH]_{2.4}^4$  and  $H[LH]_{2.4}^5$  have a wider reflection band compared to  $[\frac{LQ}{2} H_Q \frac{LQ}{2}]_{2.2}^5$ . For  $[\frac{L}{2} H][LH]_{2.4}^4$  and  $H[LH]_{2.4}^5$ , 2.4  $\mu\text{m}$  is selected as the reflectance peak wavelength, while for  $[\frac{LQ}{2} H_Q \frac{LQ}{2}]_{2.2}^5$ , 2.2  $\mu\text{m}$  is chosen as the reflectance peak wavelength.  $[\frac{L}{2} H][LH]_{2.4}^4$  and  $H[LH]_{2.4}^5$  have a wider reflection band compared to  $[\frac{LQ}{2} H_Q \frac{LQ}{2}]_{2.2}^5$ .

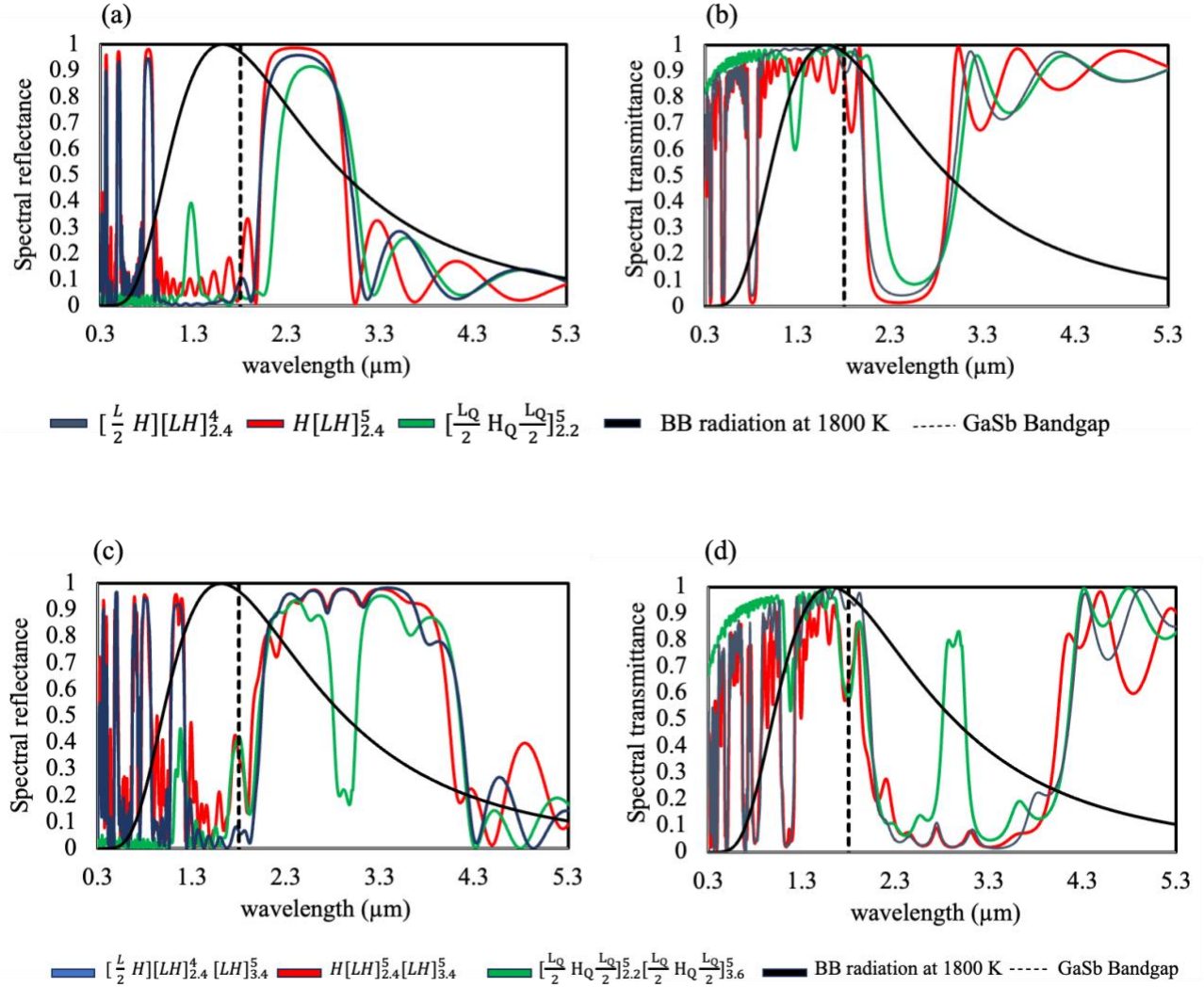


Figure 20. Normal-angle spectral (a) reflectance and (b) transmittance of the designed one stack

1DPC filters in three arrangements of  $H[LH]_{2.3}^5$ ,  $[\frac{LQ}{2} H_Q \frac{LQ}{2}]_{2.1}^5$  (quintic) and  $[\frac{L}{2} H][LH]_{2.3}^4$ .

Normal-angle (c) reflectance and (d) transmittance of the designed double stack 1DPC filters in

three arrangements of  $H[LH]_{2.4}^5[LH]_{3.4}^5$ ,  $[\frac{LQ}{2} H_Q \frac{LQ}{2}]_{2.2}^5 [\frac{LQ}{2} H_Q \frac{LQ}{2}]_{3.6}^5$  and  $[\frac{L}{2} H][LH]_{2.4}^4[LH]_{3.4}^5$

index.

The black lines in Figure 20 are the normalized radiation from a BB at a temperature of 1800 K, demonstrating the spectral match between the transmittance of the designed filters and the radiation from the emitter at the operating temperature of 1800 K. Notably, at the operating temperature of 1800 K, the peak radiation spectrum falls into the in-band region. The bandgap of the cell, which demarcates the in-band and out-of-band regions, is denoted by the vertical dotted black line.

To enhance the out-of-band reflectance, a secondary filter is stacked atop the primary filter for Cases 4 to 6, creating a double-stack filter arrangement. These stacked filter configurations feature two distinct peak positions adjusted in accordance with TPV system efficiency criteria. Figure 20 c) and 20 d) show the reflection and transmission spectra of the stacked filters. Adding a secondary filter can boost out-of-band reflectance and also impact in-band transmittance. The selection of peak positions for the secondary filter is crucial for achieving the highest TPV system efficiency. Section 4.2 demonstrates the optimization of peak positions for both the first and second stacks.  $H[LH]_{2.4}^5[LH]_{3.4}^5$  with a quarter-wave stack structure has higher reflectance compared to  $H[LH]_{2.4}^5$ , expanding the out-of-band reflectance spectrum. However, it still has a poor in-band transmittance.  $[\frac{LQ}{2} H_Q \frac{LQ}{2}]_{2.2}^5[\frac{LQ}{2} H_Q \frac{LQ}{2}]_{3.6}^5$  promises improved in-band transmission, significantly reducing local reflection peaks in the in-band region.  $[\frac{L}{2} H][LH]_{2.4}^4[LH]_{3.4}^5$  shows a reflection peak for wavelengths less than 1.3  $\mu\text{m}$ . In the range of 1.3  $\mu\text{m}$  to 1.8  $\mu\text{m}$ , where most usable photons are found, it promises a smooth transmission of light.

In Figure 20, the reflection and transmission spectra of the designed filters were presented. A notable research question arises regarding how  $\text{ZrO}_2/\text{SiO}_2$  absorbs light. The subsequent graph illustrates the percentage of light absorbed within both the in-band and out-of-band regions. Figure 21 offers a comprehensive optical performance evaluation for six filters operating under varying

emitter temperatures. The analysis segregates two regions: in-band (Figure 21 a) and out-of-band (Figure 21 b). In this graph, transmittance is the percentage of in-band and out-of-band energy transmitted from the filter ( $\bar{T}_{\text{in-band}}^P$  for Fig 15a,  $\bar{T}_{\text{out-of-band}}^P$  for Fig 15b). reflectance is the percentage of in-band/out-of-band energy that is reflected by the filter ( $\bar{R}_{\text{in-band}}^P / \bar{R}_{\text{out-of-band}}^P$ ) and absorptance is the percentage of in-band/out-of-band energy that is absorbed by the filter ( $\bar{A}_{\text{in-band}}^P / \bar{A}_{\text{out-of-band}}^P$ ). Observably, as the operating temperature rises, the in-band absorption escalates while the out-of-band absorption recedes. Notably, a minimal absorption ( $\bar{A}_{\text{in-band}}^P$ ) of 3.5% is attained at an operating temperature of 2000 K over the in-band region. Raising the operating temperature causes the peak BB radiation position to shift toward higher energy wavelengths known as a blue shift. As a result, more light falls into the in-band region, and less radiation has wavelengths greater than 7  $\mu\text{m}$ , where  $\text{SiO}_2$  NPs absorb light. While dense  $\text{ZrO}_2$  layer have minimal absorption, absorption in the  $\text{SiO}_2$  layers increase for wavelengths above 7  $\mu\text{m}$  (Figure. 21 a). For lower operating emitter temperatures, where more of the radiated energy is in the out-of-band region, the absorption is relatively larger than cases with higher operating emitter temperature.

Overall, it's clear that the behavior of 1D PC optical filters varies between the in-band and out-of-band regions in all six cases. As the operating temperature increases, these filters allow more in-band light to pass through while reflecting more out-of-band light. Comparing Cases 1 to 3, it is evident that Case 2 shows better in-band transmission with lower out-of-band reflection at lower operating temperatures. However, as the temperature rises, Case 3 surpasses Case 2 in in-band transmission while maintaining acceptable out-of-band reflection. Case 2 is characterized by a continuous and gradual change in refractive index, while Case 1 and case 3 exhibits a sudden and

sharp transition. The 1DPC with a smoothly changing refractive index facilitate the passage of electromagnetic waves more effectively compared to those with abrupt changes. As a simple analogy, This can be likened to the difference between climbing a wall and using stairs to ascend from one floor to another. The graded index structure acts as a ‘staircase’, allowing for a smoother transmission of electromagnetic waves within in-band region.

Comparing the first three cases (Case 1 to 3) with the second three cases (Case 4 to 6), a general improvement in out-of-band reflection is observed. However, these double-stack structures (Case 4 to 6) have less in-band transmission. In simpler terms, a one-dimensional photonic crystal (1DPC) initially creates a bandgap, preventing specific wavelengths from passing through the filter. Introducing a secondary filter with its own bandgap broadens the reflection spectrum, effectively blocking a wider range of out-of-band waves.

At the operating temperature of 1800 K, Case 4 has the highest out-of-band reflection. However, because of its poor in-band transmission, it is anticipated that Case 6 and Case 5, with better in-band transmission, could potentially offer higher TPV system efficiency. In the next section, the third objective is explored, which centers on the application of the suggested 1DPC filters in the TPV system. The assessment of these optical filters, based on TPV system efficiency and electrical power output, will reveal the trade-off between in-band transmission and out-of-band reflection.

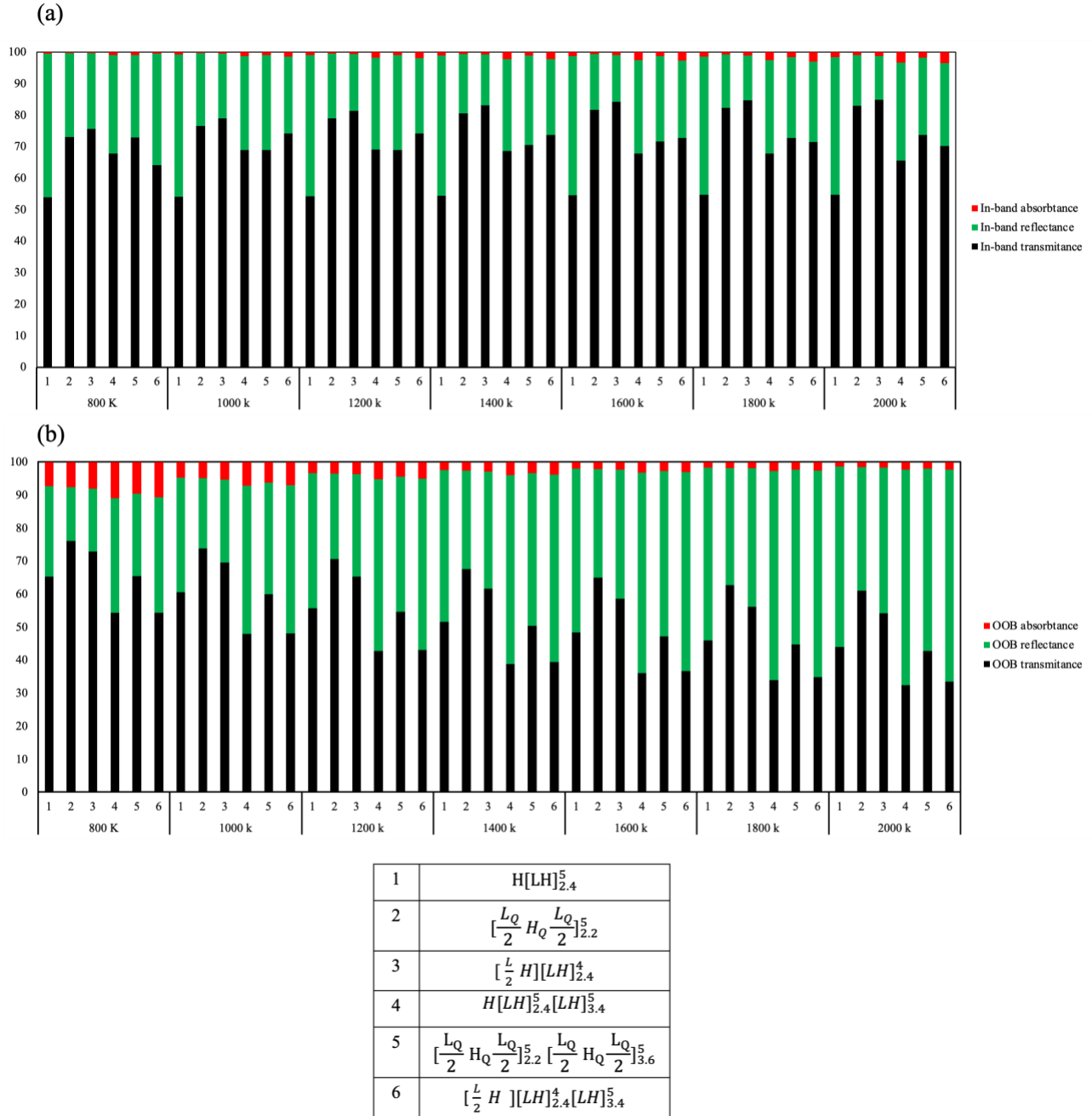


Figure 21. Optical behavior of six designed filters in terms of transmittance, reflectance, and absorbance for (a) in-band region and (b) out-of-band region at different emitter temperatures.

## 4.2 Evaluation of TPV System with the Designed Optical Filters

In the prior section, an optical analysis of 1DPC optical filters were presented. In this section the performance of the 1DPC optical filters with  $H[LH]_{\lambda_1}^5$ ,  $[\frac{LQ}{2} H_Q \frac{LQ}{2}]_{\lambda_1}^5$ ,  $[\frac{L}{2} H][LH]_{\lambda_1}^4$ ,  $H[LH]_{\lambda_1}^5[LH]_{\lambda_2}^5$ ,  $[\frac{LQ}{2} H_Q \frac{LQ}{2}]_{\lambda_1}^5 [\frac{LQ}{2} H_Q \frac{LQ}{2}]_{\lambda_2}^5$  and  $[\frac{L}{2} H][LH]_{\lambda_1}^4[LH]_{\lambda_2}^5$  configurations, which were described earlier, will be assessed. Additionally, suggestions for optimum peak wavelength positions based on TPV system efficiency are provided.

Figure 22 presents the spectral efficiency, TPV system efficiency, and electrical power output for all six 1DPC filters at different peak wavelength positions. The details of the graph are discussed as follows:

Figures 22 a, 22 c and 22 e detail the spectral efficiency, TPV system efficiency and power output of the TPV system for various peak positions for one stack filters. The first peak wavelength positions ( $\lambda_1$ ) are 2.2  $\mu\text{m}$  for the quarter-wave structure (case 2) and 2.4  $\mu\text{m}$  for the quarter-wave stack (case 1) and modified quarter-wave structure (case 3). These graphs detail the optimization of second peak positions ( $\lambda_2$ ) for double stack filters based on the spectral efficiency, TPV system efficiency and power output of the TPV system.

Figures 22 b, 22 d and 22 f introduce a comparison of three double stack filters of  $H[LH]_{2.4}^5[LH]_{\lambda_2}^5$ ,  $[\frac{LQ}{2} H_Q \frac{LQ}{2}]_{2.2}^5 L_Q [\frac{LQ}{2} H_Q \frac{LQ}{2}]_{\lambda_2}^5$  and  $[\frac{L}{2} H][LH]_{2.4}^4[LH]_{\lambda_2}^5$  that incorporates two filters with different reflectance peak positions, increasing the reflection spectrum's out-of-band range. During the optimization process for  $\lambda_2$ , the initial peak position is held constant at 2.2  $\mu\text{m}$  for the quintic structure and 2.4  $\mu\text{m}$  for the quarter-stack and modified quarter-stack. The second peak ( $\lambda_2$ )

undergoes shifts for optimization, focusing on maximizing spectral efficiency, TPV system efficiency and power output.

Finally, the optimization outcomes for the dual stack filter, in relation to the quintic stack, quarter-stack and modified quarter-stack, are presented in Table 3. The data suggests that

$[\frac{LQ}{2} H_Q \frac{LQ}{2}]_{2.2}^5 L_Q [\frac{LQ}{2} H_Q \frac{LQ}{2}]_{3.6}^5$  with maintains high power output levels of  $7.15 \text{ W/cm}^2$  compared

to  $H[LH]_{2.4}^5 [LH]_{3.4}^5$  which has a power output of  $5.9 \text{ W/cm}^2$ . Notably, spectral and TPV system

efficiency of both are 44% and 22%, respectively.

$[\frac{L}{2} H][LH]_{2.4}^4 [LH]_{3.4}^5$  attains a peak spectral efficiency of 47% and TPV system efficiency of 24%

when  $\lambda_2$  is set to  $3.4 \text{ }\mu\text{m}$ , correlating with a power output of  $6.95 \text{ W/m}^2$ .

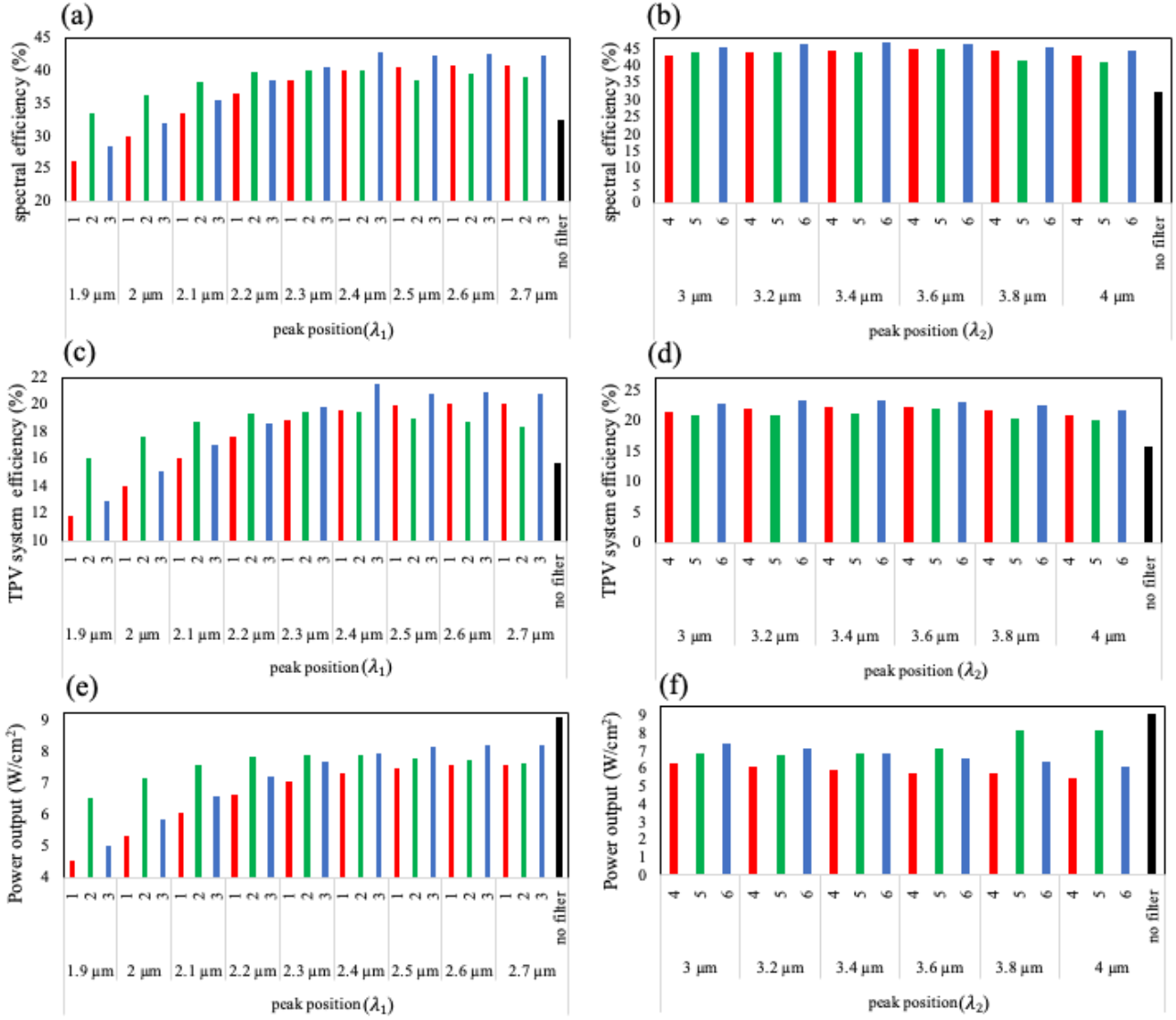


Figure 22. Optimizing spectral efficiency (a), (b) and TPV system efficiency (c), (d) and power output (f) at 1800K emitter temperature with varying peak positions in the following cases: (1)

$$\begin{aligned}
 & \text{H}[\text{LH}]_{\lambda_1}^5, (2) \left[ \frac{L_Q}{2} \text{H}_Q \frac{L_Q}{2} \right]_{\lambda_1}^5, (3) \left[ \frac{L}{2} \text{H} \right] [\text{HL}]_{\lambda_1}^4, (4) \text{H}[\text{LH}]_{2.4}^5 [\text{LH}]_{\lambda_2}^5, (5) \\
 & \left[ \frac{L_Q}{2} \text{H}_Q \frac{L_Q}{2} \right]_{2.2}^5 L_Q \left[ \frac{L_Q}{2} \text{H}_Q \frac{L_Q}{2} \right]_{\lambda_2}^5 \text{ and } (6) \left[ \frac{L}{2} \text{H} \right] [\text{LH}]_{2.4}^4 [\text{LH}]_{\lambda_2}^5.
 \end{aligned}$$

Table 3. Comparison between six designs of 1DPC filters and case with no filter at 1800 K.

Notation	Structure	Reflectance Peak position	$\eta_{\text{spec}}$ (%)	$T_{\text{in-band}}^{\text{P}}$	$R_{\text{out-of-band}}^{\text{P}}$	$\eta_{\text{TPV}}$ (%)	$P_{\text{PV}}$ (w/cm <sup>2</sup> )
No Filter	-	-	32.3	100	0	15.6	9.1
$\text{H}[\text{LH}]_{2.3}^5$	Quarter-stack, single	2.4 $\mu\text{m}$	39.2	79.8	43.3	19.5	7.3
$[\frac{L_Q}{2} \text{H}_Q \frac{L_Q}{2}]_{2.2}^5$	Quintic-stack, single	2.2 $\mu\text{m}$	39.8	87.7	38	19.3	8.1
$[\frac{L}{2} \text{H}][\text{HL}]_{2.4}^4$	Modified quarter stack, single	2.4 $\mu\text{m}$	42	86.4	42.9	21	7.9
$\text{H}[\text{LH}]_{2.4}^5[\text{LH}]_{3.4}^5$	modified quarter stack, double	2.4 $\mu\text{m}$ , 3.4 $\mu\text{m}$	44.5	63.6	63.4	22.2	5.9
$[\frac{L_Q}{2} \text{H}_Q \frac{L_Q}{2}]_{2.2}^5 \text{L}_Q [\frac{L_Q}{2} \text{H}_Q \frac{L_Q}{2}]_{3.6}^5$	quintic stack, double	2.2 $\mu\text{m}$ , 3.6 $\mu\text{m}$	44.9	78	54	22.1	7.15
$[\frac{L}{2} \text{H}][\text{HL}]_{2.4}^4[\text{HL}]_{3.4}^5$	Modified quarter stack, double	2.4 $\mu\text{m}$ , 3.4 $\mu\text{m}$	47	74	62	24	6.9

## 5 Discussion

In the previous chapter, the examination of various 1DPC arrangements clarified that incorporating a graded layer offers advantages, particularly with increased in-band transmittance.

The selection of a filter depends on system constraints such as cost, space and scale of the project. In aerospace applications, prioritizing higher system efficiency, even at the cost of reduced power output, may lean towards selection of a modified 1DPC, such as Case 6. On the other hand, in large-scale TPV systems with no space limits where maximizing power output is essential, selection of a graded filter, similar to Case 5, might become advantageous by transmitting more in-band energy.

However, it's important to note that currently, there are no commercially available filters that can match the reflectance and transmittance spectra of the proposed filters in this study. The few existing filters that come close often lack high power output promised in this work. However, presented 1DPC filter have significant challenges in their fabrication. Porosity directly affects refractive index. Tuning the porosity of the materials studied here, like  $\text{SiO}_2$  and  $\text{ZrO}_2$ , is crucial. Achieving a graded structure, specially creating precise graded index profiles throughout the PC, proves to be difficult. The complexity arises from the intricate control needed for the continuous change in the refractive index profile over many periods in the PC [39], [106]. As previously discussed, fabricating graded-index profiles in optical filters for industrial use remains a significant challenge. Therefore, a cost analysis for the optical filters introduced optical filters in this study could pave the road for commercialization and realization of market value of these 1DPC filter.

The challenges in making graded-index profiles for optical filters, as previously discussed, make them hard to use widely in industry. Therefore, conducting a cost analysis for the optical filters introduced in this study is crucial. Such an analysis could illuminate the path towards commercialization, showcasing the market value of these 1DPC filters. It's essential to understand and quantify the manufacturing complexities, material costs, and scalability factors associated with these filters. By providing a detailed financial overview, this research can bridge the gap between theoretical innovation and practical application, potentially leading to more widespread use of these advanced optical filters in various industries. This step is vital for realizing the commercial potential of 1DPC filters and facilitating their transition from laboratory concepts to marketable products [122].

As we discussed earlier, making graded-index profiles in the optical filter for industrial use is still a challenge. As a result, the optical filters introduced in this study may not be the most cost-effective option right now. However, recent reports in the literature suggest new methods are emerging. Future efforts should center on using these techniques to develop a straightforward and economical way to produce graded index profiles and optical filters. This would make them more practical for use in various TPV systems.

In the preceding chapter, all simulations factored in material absorption. Through careful selection of  $ZrO_2$  and  $SiO_2$  materials, it was observed that absorption can be minimized to 4% at operating temperatures above 1800 K, rendering it negligible. This chapter employs a theoretical approach with simplified assumptions about the system to provide an overview of TPV system performance equipped with a front side filter. In this approach, absorption is disregarded to specifically examine the analytical effects of in-band transmission and out-of-band reflection, two crucial parameters. This method enables an assessment of the TPV system's maximum potential under the assumption

of no absorption. In this scenario, the filter either reflects or transmits light based on wavelength. Segmenting the spectrum into in-band and out-of-band regions allows the creation of a plot for the TPV system. To generate Figure 23 for spectral and TPV system efficiency, Equations 24 to 26 are applied.

In Figures 17 a and 17 b the spectral efficiency and TPV system efficiency are plotted as a function of  $R_{\text{out-of-band}}^P$  and  $T_{\text{in-band}}^P$  for the case when the BB emitter is at 1800 K, the view factor is 1, and the absorption within the filter is neglected. Different filters can be mapped onto these plots such that their performance can be compared. The chart displays a theoretical TPV efficiency of 46% and spectral efficiency of 100 % for 100%  $T_{\text{in-band}}^P$  and  $R_{\text{out-of-band}}^P$ . The contour lines on the graph represent equivalent TPV system efficiency values. As expected, the spectral and TPV system efficiencies increase as  $R_{\text{out-of-band}}^P$  and  $T_{\text{in-band}}^P$  increase. The plot can be used as a “map” that shows how improving the optical parameters of the filter can improve the spectral efficiency and TPV system efficiency. These “maps” are specific to the temperature of the emitter and the type of PV cell and the emitter-to-PV-cell view factor (similar figures can be made for a given set of the type of PV cell, emitter temperature, and emitter-to-PV cell view factor, which makes it practical for any TPV geometry).

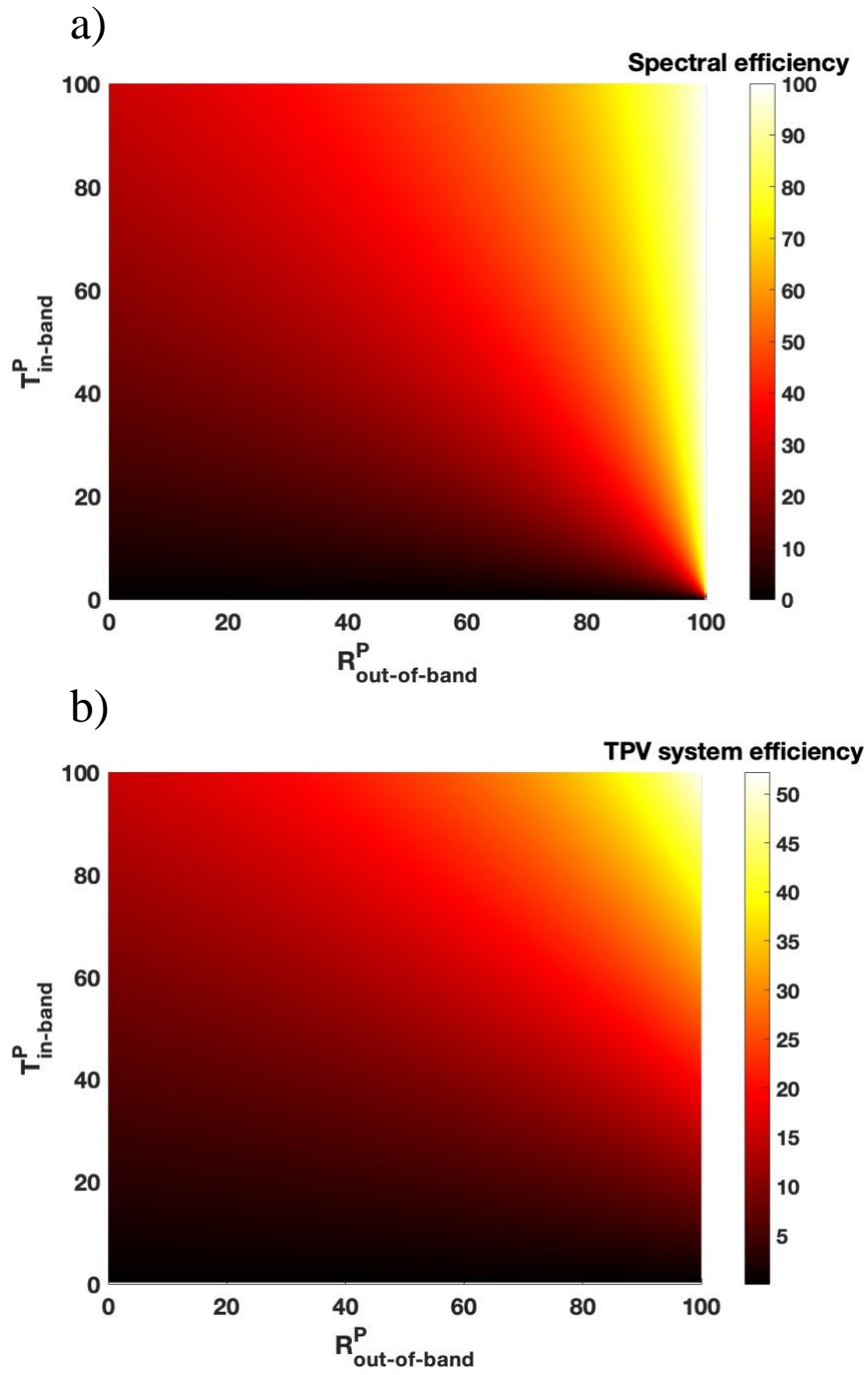


Figure 23. (a) Spectral efficiency and (b) TPV system efficiency as a function of the in-band transmittance and out-of-band reflectance when the emitter is at a temperature of 1800 K and absorption in the filter is neglected.

Since the introduction of the idea of using a 1DPC optical filter in TPV systems, various studies have aimed to optimize 1DPC with different structures or material selections. In Table 4, been attempted to compile numerical and experimental studies on TPV with a 1DPC optical filter. The second and third columns present commonly chosen PV cell and emitter temperatures. GaSb is the most frequently reported PV cell, and the emitter temperature is typically 1800 K. Spectral efficiency, power output, TPV system efficiency, in-band transmittance, and out-of-band reflectance are detailed in the next column for comparison. It is essential to note that different numerical simulation and experimental approaches were employed in these studies, impacting the reported results. The common structure used in the filter is also mentioned. In this thesis, a suggested TPV system efficiency is 24%, with a spectral efficiency of 47% and electrical power output of 6.95 W/cm<sup>2</sup>. This contrasts with reported spectral efficiencies of 74% for 1D TiO<sub>2</sub>/SiO<sub>2</sub>, 64% for 1D TiO<sub>2</sub>/GO, and 75% for 1D Ge/MgF<sub>2</sub> using the TMM method. It's important to note that these reported values involve simplified assumptions in material properties, neglecting absorption, normal angle simulation, or narrower spectral analysis. This study proposes a more detailed simulation approach as explained in both optical and TPV system.

Table 4. Designed and fabricated filter in TPV

Filter design	PV cell	T (K)	$\eta_{\text{spec}}$	PPV (w/cm <sup>2</sup> )	$\eta_{\text{TPV}}$	Structure	Method
1D SiO <sub>2</sub> /ZrO <sub>2</sub> NP	GaSb	1800	47	6.95	24	$\frac{L}{2}H[LH]_{2.4}^4 \cdot [LH]_{3.4}^5$	Numerical - FEM
1D SiO <sub>2</sub> /ZrO <sub>2</sub> NP	GaSb	1800	44	7.15	21	$\frac{L}{2}H[LH]_{2.2}^4 \cdot [LH]_{3.6}^5$	Numerical - FEM
ZrO <sub>2</sub> /ZrO <sub>2</sub> aerogel [81]	GaSb	1800	46	8.5	33	$\frac{L}{2}H[LH]_{\lambda_1}^4 \cdot [LH]_{\lambda_2}^5$	Numerical – FEM [123] and MCM
1D Si/SiO <sub>2</sub> [41]	GaSb	1800	40	7.5	-	$[L/2H][LH]^4$	Analytical
1D Si/SiO <sub>2</sub> [40]	GaSb	1800	-	6	42	$[L/2][HL]^4[H/2]$	Analytical[124], GAOS[125]
1D TiO <sub>2</sub> /GO [82]	GaSb	1800	64	8.2	39	$\frac{L}{2}H[LH]_{\lambda_1}^4 \cdot [LH]_{\lambda_2}^4 [L\frac{H}{2}]$	TMM [126]
1D ZnS/MgF <sub>2</sub> with Au [75] or Ag [74]	Si, Ge	2500	-	-	-	$[HL]^P H M H [LH]^P$	Characteristic Matrix Method [127] [128]
1D HfF <sub>4</sub> /SiH and SiH/SiO <sub>2</sub> [129], [130]	-	-	-	-	-	$L[HL]^4$	Fabrication, RF magnetron sputtering
1D TiO <sub>2</sub> /SiO <sub>2</sub> [131]	GaSb	1800	74	-	-	$[LH]^P$	TMM [126]
1D Si/SiON [83]	GaSb	1800	60.5	6.8	31	$[L/2H][LH]^4$	Fabrication - LPCVD [132]
1D Si/SiO <sub>2</sub> [83]	GaSb	1800	52.8	7.2	36	$[L/2H][LH]^4$	Fabrication - LPCVD [132]
1D Si/SiO <sub>2</sub> [84]	GaSb	1600	53	3.9	26	$[L/2 H][LH]^3, [LH]^4$	TMM [126] Fabrication-PVD
1D Si/SiO <sub>2</sub> [85]	GaSb	1800	55.2	8.7	-	$[1+\Delta_1][L/2HL/2][L/2HL/2]^3[1+\Delta_2][L/2HL/2]$	TMM [126] Fabrication - reactive magnetron sputtering
1D Si/SiO <sub>2</sub> [88]	GaSb	1500	33.5	-	-	$[HL]^4$	RCWA [133]

1D Si/SiO <sub>2</sub> [86]	GaSb	1500	-	-	-	[LH] <sup>n</sup> LL[HL] <sup>n</sup>	TMM [126]
1D Si/SiO <sub>2</sub> [91]	InGaSb	1800	38	6.6	-	$\frac{L}{2}H[LH]_{2.21}^4 \cdot \frac{L}{2}H[LH]_{3.6}^4$	RCWA [133]
1D Ge/ MgF <sub>2</sub> [92]	GaSb	1800	75	-	-	[L/2][HL] <sup>4</sup>	TMM [126] and Pattern search (PS)
1D porous Si [134]	-	-	-	-	-	L[HL] <sup>7</sup> HH[LH] <sup>7</sup> L	Fabrication - physical vapor deposition (PVD) and electron beam
1D Ag/SiO <sub>2</sub> [87]	GaSb	1500	66.5			(D/2) (MD) <sup>n</sup> (D/2)	TMM

## 6 Conclusion

In conclusion, despite the significant potential of TPV systems in renewable energy applications, the challenge of spectral and directional control of thermal radiation reaching PV cells persists. This study explored the enhancement of in-band transmission in TPV systems using 1DPC filters with graded refractive index profiles. The research focused on optimizing these structures explicitly for TPV applications, comparing them with quarter-stack and modified quarter-stack configurations.

The objectives of the thesis were to conduct a comparative study of 1DPC graded index structure, develop optimization strategies for TPV systems. A numerical approach utilizing COMSOL was employed to analyze the optical behavior of 1D  $\text{ZrO}_2/\text{SiO}_2$  PCs in various configurations.

The structure of the thesis included an introduction to TPV, design, simulation, and validation of the proposed 1DPC optical filter, and performance analysis. The research aimed to enhance TPV system performance using 1DPC structures as optical filters. The analysis revealed that a dual-stack graded filter demonstrated promising results with 74% in-band transmittance and 55% out-of-band reflectance at an emitter temperature of 2000 K. Minimal absorption of 3.5 % were promised in the simulation of corresponding optical filter.

Despite challenges in balancing in-band transmittance and out-of-band reflectance, the optimized filter structure, a modified quarter-stack profile with two filters of varied peak positions, showed potential as a photon recycling apparatus. In an ideal TPV system implementation, this optimized

filter yielded a system efficiency of 24% and a power density of 6.9 W/cm<sup>2</sup>, providing valuable insights into the limits of TPV systems.

## 7 References

- [1] “Primary energy consumption by source, World.” [Online]. Available: <https://ourworldindata.org/grapher/primary-sub-energy-source>
- [2] “Statistical Review of World Energy.” [Online]. Available: <https://www.energyinst.org/statistical-review/resources-and-data-downloads>
- [3] “Net-Zero Emissions by 2050.” [Online]. Available: <https://www.canada.ca/en/services/environment/weather/climatechange/climate-plan/net-zero-emissions-2050.html>
- [4] White, David C., Bruce D. Wedlock, and John Blair, “Recent advances in thermal energy conversion,” in *15th Annual Proceedings*, 1961.
- [5] L. Broman, “Thermophotovoltaics bibliography,” *Prog. Photovolt. Res. Appl.*, vol. 3, no. 1, pp. 65–74, 1995, doi: 10.1002/pip.4670030108.
- [6] Kolm H H, “Solar-battery power source,” MIT Lincoln Laboratory, Lexington, MA, Quarterly Progress Report, 1956.
- [7] R. E. Nelson, “A brief history of thermophotovoltaic development,” *Semicond. Sci. Technol.*, vol. 18, no. 5, pp. S141–S143, May 2003, doi: 10.1088/0268-1242/18/5/301.
- [8] John J Werth, “Thermo-photovoltaic converter with radiant energy reflective means,” US3331707A [Online]. Available: <https://patentimages.storage.googleapis.com/94/8a/9a/ad3f56910a32ce/US3331707.pdf>
- [9] R. M. Swanson, “A proposed thermophotovoltaic solar energy conversion system,” *Proc. IEEE*, vol. 67, no. 3, pp. 446–447, 1979, doi: 10.1109/PROC.1979.11270.
- [10] M. W. Edburn, “Analytical evaluation of a solar thermophotovoltaic (TPV) converter,” *Sol. Energy*, vol. 24, no. 4, pp. 367–371, 1980, doi: 10.1016/0038-092X(80)90299-6.
- [11] B. S. Good and D. L. Chubb, “Effects of geometry on the efficiency of TPV energy conversion,” in *Third NREL Conference on thermophotovoltaic generation of electricity*, Colorado Springs, Colorado (USA): ASCE, 1997, pp. 487–503. doi: 10.1063/1.53285.
- [12] B. S. Good and D. L. Chubb, “A comparison of planar and cylindrical thermophotovoltaic energy conversion systems,” in *IECEC-97 Proceedings of the Thirty-Second Intersociety Energy Conversion Engineering Conference (Cat. No.97CH6203)*, Honolulu, HI, USA: IEEE, 1997, pp. 1113–1118 vol.2. doi: 10.1109/IECEC.1997.661926.
- [13] Andrew Joseph PonecJustin BriggsDavid BiermanTarun Narayan, “System and method for a solid-state thermal battery,” US20210143446A1
- [14] Dr. Veronika Stelmakh and Dr. Walker Chan, “Mesodyne.” [Online]. Available: <https://mesodyne.com/>
- [15] Carlos Bermejo, “Thermophoton (2021).” [Online]. Available: <https://www.thermophoton.com/>
- [16] “TPV-13.” [Online]. Available: <https://www.tpv-13.org/>
- [17] “TPV-14.” [Online]. Available: <https://www.tpv-14.org/>
- [18] “Antora Energy’s battery. The startup’s pilot is up and running in Fresno, California. Photographer: Kelly Petersen.” [Online]. Available: <https://www.bloomberg.com/news/articles/2023-09-12/bill-gates-backed-startup-pilots-unique-battery-to-help-heavy-industry?srnd=undefined&sref=jPQnHIEd#xj4y7vzkg>
- [19] Z. Utlu, “Thermophotovoltaic applications in waste heat recovery systems: example of GaSb cell,” *Int. J. Low-Carbon Technol.*, vol. 15, no. 2, pp. 277–286, May 2020, doi: 10.1093/ijlct/ctz049.
- [20] Alejandro Datas Medina, “Development of Solar Thermophotovoltaic Systems,” POLITÉCNICA DE MADRID, 2011.
- [21] Z. Zhou, E. Sakr, Y. Sun, and P. Bermel, “Solar thermophotovoltaics: reshaping the solar spectrum,” *Nanophotonics*, vol. 5, no. 1, pp. 1–21, Jun. 2016, doi: 10.1515/nanoph-2016-0011.

- [22] C. Amy, H. R. Seyf, M. A. Steiner, D. J. Friedman, and A. Henry, “Thermal energy grid storage using multi-junction photovoltaics,” *Energy Environ. Sci.*, vol. 12, no. 1, pp. 334–343, 2019, doi: 10.1039/C8EE02341G.
- [23] C. Amy *et al.*, “Thermal energy grid storage: Liquid containment and pumping above 2000 °C,” *Appl. Energy*, vol. 308, p. 118081, Feb. 2022, doi: 10.1016/j.apenergy.2021.118081.
- [24] Bauer T., “Section 8.3.2 of the book,” in *Thermophotovoltaics: basic principles and critical aspects of system design*, Springer Science & Business Media, 2011.
- [25] A. Datas, “Bifacial Thermophotovoltaic Energy Conversion,” *ACS Photonics*, Feb. 2023, doi: 10.1021/acsp Photonics.2c01839.
- [26] H. Daneshvar, R. Prinja, and N. P. Kherani, “Thermophotovoltaics: Fundamentals, challenges and prospects,” *Appl. Energy*, vol. 159, pp. 560–575, Dec. 2015, doi: 10.1016/j.apenergy.2015.08.064.
- [27] P. Bermel *et al.*, “Design and global optimization of high-efficiency thermophotovoltaic systems,” *Opt. Express*, vol. 18, no. S3, p. A314, Sep. 2010, doi: 10.1364/OE.18.00A314.
- [28] A. LaPotin *et al.*, “Thermophotovoltaic efficiency of 40,” *Nat. Lond.*, vol. 604, no. 7905, pp. 287–291, 2022, doi: 10.1038/s41586-022-04473-y.
- [29] C. Amy, M. Pishahang, C. C. Kelsall, A. LaPotin, and A. Henry, “High-temperature Pumping of Silicon for Thermal Energy Grid Storage,” *Energy*, vol. 233, p. 121105, Oct. 2021, doi: 10.1016/j.energy.2021.121105.
- [30] C. C. Kelsall, K. Buznitsky, and A. Henry, “Technoeconomic Analysis of Thermal Energy Grid Storage Using Graphite and Tin,” 2021, doi: 10.48550/ARXIV.2106.07624.
- [31] M. S. Ziegler *et al.*, “Storage Requirements and Costs of Shaping Renewable Energy Toward Grid Decarbonization,” *Joule*, vol. 3, no. 9, pp. 2134–2153, Sep. 2019, doi: 10.1016/j.joule.2019.06.012.
- [32] N. A. Sepulveda, J. D. Jenkins, A. Edington, D. S. Mallapragada, and R. K. Lester, “The design space for long-duration energy storage in decarbonized power systems,” *Nat. Energy*, vol. 6, no. 5, pp. 506–516, Mar. 2021, doi: 10.1038/s41560-021-00796-8.
- [33] B. Wernsman *et al.*, “Greater Than 20% Radiant Heat Conversion Efficiency of a Thermophotovoltaic Radiator/Module System Using Reflective Spectral Control,” *IEEE Trans. Electron Devices*, vol. 51, no. 3, pp. 512–515, Mar. 2004, doi: 10.1109/TED.2003.823247.
- [34] T. Burger, B. Roy-Layinde, R. Lentz, Z. J. Berquist, S. R. Forrest, and A. Lenert, “Semitransparent thermophotovoltaics for efficient utilization of moderate temperature thermal radiation,” *Proc. Natl. Acad. Sci.*, vol. 119, no. 48, p. e2215977119, Nov. 2022, doi: 10.1073/pnas.2215977119.
- [35] W. H. Southwell, “Omnidirectional mirror design with quarter-wave dielectric stacks,” *Appl. Opt.*, vol. 38, no. 25, p. 5464, Sep. 1999, doi: 10.1364/AO.38.005464.
- [36] M. Rostami, A. Pirvaram, N. Talebzadeh, and P. G. O’Brien, “Numerical evaluation of one-dimensional transparent photonic crystal heat mirror coatings for parabolic dish concentrator receivers,” *Renew. Energy*, vol. 171, pp. 1202–1212, Jun. 2021, doi: 10.1016/j.renene.2021.03.007.
- [37] M. Rostami, N. Talebzadeh, and P. G. O’Brien, “Transparent Photonic Crystal Heat Mirrors for Solar Thermal Applications,” *Energies*, vol. 13, no. 6, p. 1464, Mar. 2020, doi: 10.3390/en13061464.
- [38] U. Ortabasi, “Rugate Technology For Thermophotovoltaic (TPV) Applications: A New Approach To Near Perfect Filter Performance,” in *AIP Conference Proceedings*, Rome (Italy): AIP, 2003, pp. 249–258. doi: 10.1063/1.1539381.
- [39] S. Callard, A. Gagnaire, and J. Joseph, “Fabrication and characterization of graded refractive index silicon oxynitride thin films,” *J. Vac. Sci. Technol. Vac. Surf. Films*, vol. 15, no. 4, pp. 2088–2094, Jul. 1997, doi: 10.1116/1.580614.
- [40] I. Celanovic, F. O’Sullivan, M. Ilak, J. Kassakian, and D. Perreault, “Design and optimization of one-dimensional photonic crystals for thermophotovoltaic applications,” *Opt. Lett.*, vol. 29, no. 8, p. 863, Apr. 2004, doi: 10.1364/OL.29.000863.
- [41] I. Celanovic, F. O’Sullivan, N. Jovanovic, M. Qi, and J. G. Kassakian, “1D and 2D photonic crystals for thermophotovoltaic applications,” presented at the Photonics Europe, R. M. De La Rue,

- P. Viktorovitch, C. M. Sotomayor Torres, and M. Midrio, Eds., Strasbourg, France, Sep. 2004, p. 416. doi: 10.1117/12.545539.
- [42] N. A. Pfiester and T. E. Vandervelde, “Selective emitters for thermophotovoltaic applications,” *Phys. Status Solidi A*, vol. 214, no. 1, p. 1600410, Jan. 2017, doi: 10.1002/pssa.201600410.
- [43] A. Narayanaswamy and G. Chen, “Thermal emission control with one-dimensional metallodielectric photonic crystals,” *Phys. Rev. B*, vol. 70, no. 12, p. 125101, Sep. 2004, doi: 10.1103/PhysRevB.70.125101.
- [44] D. L. C. Chan, M. Soljačić, and J. D. Joannopoulos, “Thermal emission and design in one-dimensional periodic metallic photonic crystal slabs,” *Phys. Rev. E*, vol. 74, no. 1, p. 016609, Jul. 2006, doi: 10.1103/PhysRevE.74.016609.
- [45] I. Celanovic, N. Jovanovic, and J. Kassakian, “Two-dimensional tungsten photonic crystals as selective thermal emitters,” *Appl. Phys. Lett.*, vol. 92, no. 19, p. 193101, May 2008, doi: 10.1063/1.2927484.
- [46] V. Rinnerbauer *et al.*, “High-temperature stability and selective thermal emission of polycrystalline tantalum photonic crystals,” *Opt. Express*, vol. 21, no. 9, p. 11482, May 2013, doi: 10.1364/OE.21.011482.
- [47] J. G. Fleming, S. Y. Lin, I. El-Kady, R. Biswas, and K. M. Ho, “All-metallic three-dimensional photonic crystals with a large infrared bandgap,” *Nature*, vol. 417, no. 6884, pp. 52–55, May 2002, doi: 10.1038/417052a.
- [48] S. Y. Lin, J. Moreno, and J. G. Fleming, “Three-dimensional photonic-crystal emitter for thermal photovoltaic power generation,” *Appl. Phys. Lett.*, vol. 83, no. 2, pp. 380–382, Jul. 2003, doi: 10.1063/1.1592614.
- [49] T. A. Walsh, J. A. Bur, Y.-S. Kim, T.-M. Lu, and S.-Y. Lin, “High-temperature metal coating for modification of photonic band edge position,” *J. Opt. Soc. Am. B*, vol. 26, no. 7, p. 1450, Jul. 2009, doi: 10.1364/JOSAB.26.001450.
- [50] J. D. Joannopoulos, P. R. Villeneuve, and S. Fan, “Photonic crystals,” *Solid State Commun.*, vol. 102, no. 2–3, pp. 165–173, Apr. 1997, doi: 10.1016/S0038-1098(96)00716-8.
- [51] T. D. Rahmlow, D. M. DePoy, P. M. Fourspring, H. Ehsani, J. E. Lazo-Wasem, and E. J. Gratrix, “Development of Front Surface, Spectral Control Filters with Greater Temperature Stability for Thermophotovoltaic Energy Conversion,” in *AIP Conference Proceedings*, Madrid (Spain): AIP, 2007, pp. 59–67. doi: 10.1063/1.2711720.
- [52] Jin Hwan Kim, S. M. Jung, and M. W. Shin, “High-temperature degradation of one-dimensional metallodielectric (W/SiO<sub>2</sub>) photonic crystal as selective thermal emitter for thermophotovoltaic system,” *Opt. Mater.*, vol. 72, pp. 45–51, Oct. 2017, doi: 10.1016/j.optmat.2017.05.041.
- [53] R. Sakakibara *et al.*, “Practical emitters for thermophotovoltaics: a review,” *J. Photonics Energy*, vol. 9, no. 03, p. 1, Feb. 2019, doi: 10.1117/1.JPE.9.032713.
- [54] E. Vadiee *et al.*, “Temperature dependence of GaSb and AlGaSb solar cells,” *Curr. Appl. Phys.*, vol. 18, no. 6, pp. 752–761, Jun. 2018, doi: 10.1016/j.cap.2018.03.007.
- [55] J. Van Der Heide, N. E. Posthuma, G. Flamand, W. Geens, and J. Poortmans, “Cost-efficient thermophotovoltaic cells based on germanium substrates,” *Sol. Energy Mater. Sol. Cells*, vol. 93, no. 10, pp. 1810–1816, Oct. 2009, doi: 10.1016/j.solmat.2009.06.017.
- [56] B. Lee *et al.*, “Air-Bridge Si Thermophotovoltaic Cell with High Photon Utilization,” *ACS Energy Lett.*, vol. 7, no. 7, pp. 2388–2392, Jul. 2022, doi: 10.1021/acseenergylett.2c01075.
- [57] R. Ginige, “The Design, Fabrication and Evaluation of InGaAs/InP TPV Cells for Commercial Applications,” in *AIP Conference Proceedings*, Rome (Italy): AIP, 2003, pp. 354–362. doi: 10.1063/1.1539390.
- [58] A. W. Bett and O. V. Sulima, “GaSb photovoltaic cells for applications in TPV generators,” *Semicond. Sci. Technol.*, vol. 18, no. 5, pp. S184–S190, May 2003, doi: 10.1088/0268-1242/18/5/307.

- [59] K. Qiu, A. C. S. Hayden, M. G. Mauk, and O. V. Sulima, "Generation of electricity using InGaAsSb and GaSb TPV cells in combustion-driven radiant sources," *Sol. Energy Mater. Sol. Cells*, vol. 90, no. 1, pp. 68–81, Jan. 2006, doi: 10.1016/j.solmat.2005.02.002.
- [60] V. M. Andreev, V. P. Khvostikov, V. D. Rummyantsev, S. V. Sorokina, and M. Z. Shvarts, "c," in *Conference Record of the Twenty-Eighth IEEE Photovoltaic Specialists Conference - 2000 (Cat. No.00CH37036)*, Anchorage, AK, USA: IEEE, 2000, pp. 1265–1268. doi: 10.1109/PVSC.2000.916120.
- [61] O. V. Sulima, A. W. Bett, P. S. Dutta, M. G. Mauk, and R. L. Mueller, "GaSb-, InGaAsSb-, InGaSb-, InAsSbP- and Ge-TPV cells with diffused emitters," in *Conference Record of the Twenty-Ninth IEEE Photovoltaic Specialists Conference, 2002.*, New Orleans, LA, USA: IEEE, 2002, pp. 892–895. doi: 10.1109/PVSC.2002.1190723.
- [62] Q. Lu *et al.*, "InAs thermophotovoltaic cells with high quantum efficiency for waste heat recovery applications below 1000 °C," *Sol. Energy Mater. Sol. Cells*, vol. 179, pp. 334–338, Jun. 2018, doi: 10.1016/j.solmat.2017.12.031.
- [63] O. V. Sulima, "GaSb-, InGaAsSb-, InGaSb-, InAsSbP- and Ge-TPV cells for low-temperature TPV applications," in *AIP Conference Proceedings*, Rome (Italy): AIP, 2003, pp. 434–441. doi: 10.1063/1.1539398.
- [64] P. M. Fourspring, D. M. DePoy, T. D. Rahmlow Jr., J. E. Lazo-Wasem, and E. J. Gratrix, "Optical coatings for thermophotovoltaic spectral control," *Appl. Opt.*, vol. 45, no. 7, p. 1356, Mar. 2006, doi: 10.1364/AO.45.001356.
- [65] Y. X. Yeng, W. R. Chan, V. Rinnerbauer, J. D. Joannopoulos, M. Soljačić, and I. Celanovic, "Performance analysis of experimentally viable photonic crystal enhanced thermophotovoltaic systems," *Opt. Express*, vol. 21, no. S6, p. A1035, Nov. 2013, doi: 10.1364/OE.21.0A1035.
- [66] R. K. Huang, "Hybrid Back Surface Reflector GaInAsSb Thermophotovoltaic Devices," in *AIP Conference Proceedings*, Freiburg (Germany): AIP, 2004, pp. 329–336. doi: 10.1063/1.1841910.
- [67] L. B. Karlina, M. M. Kulagina, N. Kh. Timoshina, A. S. Vlasov, and V. M. Andreev, "In<sub>0.53</sub>Ga<sub>0.47</sub>As/InP conventional and inverted thermophotovoltaic cells with back surface reflector," in *AIP Conference Proceedings*, Madrid (Spain): AIP, 2007, pp. 182–189. doi: 10.1063/1.2711735.
- [68] Y. X. Yeng *et al.*, "Photonic crystal enhanced silicon cell based thermophotovoltaic systems," *Opt. Express*, vol. 23, no. 3, p. A157, Feb. 2015, doi: 10.1364/OE.23.00A157.
- [69] T. Burger, D. Fan, K. Lee, S. R. Forrest, and A. Lenert, "Thin-Film Architectures with High Spectral Selectivity for Thermophotovoltaic Cells," *ACS Photonics*, vol. 5, no. 7, pp. 2748–2754, Jul. 2018, doi: 10.1021/acsphotonics.8b00508.
- [70] A. Karalis and J. D. Joannopoulos, "'Squeezing' near-field thermal emission for ultra-efficient high-power thermophotovoltaic conversion," *Sci. Rep.*, vol. 6, no. 1, p. 28472, Jul. 2016, doi: 10.1038/srep28472.
- [71] Z. Omair *et al.*, "Ultraefficient thermophotovoltaic power conversion by band-edge spectral filtering," *Proc. Natl. Acad. Sci.*, vol. 116, no. 31, pp. 15356–15361, Jul. 2019, doi: 10.1073/pnas.1903001116.
- [72] E. J. Tervo *et al.*, "Efficient and scalable GaInAs thermophotovoltaic devices," *Joule*, vol. 6, no. 11, pp. 2566–2584, Nov. 2022, doi: 10.1016/j.joule.2022.10.002.
- [73] R. T. Kristensen, J. F. Beausang, and D. M. DePoy, "Frequency selective surfaces as near-infrared electromagnetic filters for thermophotovoltaic spectral control," 2014.
- [74] H. Höfler, H. J. Paul, W. Ruppel, and P. Würfel, "Interference filters for thermophotovoltaic solar energy conversion," *Sol. Cells*, vol. 10, no. 3, pp. 273–286, Dec. 1983, doi: 10.1016/0379-6787(83)90056-X.
- [75] F. Demichelis, E. Minetti-Mezzetti, M. Agnello, and V. Perotto, "Bandpass filters for thermophotovoltaic conversion systems," *Sol. Cells*, vol. 5, no. 2, pp. 135–141, Jan. 1982, doi: 10.1016/0379-6787(82)90023-0.

- [76] M. V. N. S. Gupta, E. Ameen, S. Unnikrishnakurup, K. Balasubramaniam, A. Veeraragavan, and B. Pesala, "Spectral filtering of sub-bandgap radiation using all-dielectric gratings for thermophotovoltaic applications," *J. Photonics Energy*, vol. 11, no. 01, Jan. 2021, doi: 10.1117/1.JPE.11.015501.
- [77] X. Wu, W. P. Mulligan, J. D. Webb, and T. J. Coutts, "TPV plasma filters based on cadmium stannate," in *AIP Conference Proceedings*, Colorado Springs, Colorado (USA): AIP, 1996, pp. 329–338. doi: 10.1063/1.49715.
- [78] T. D. Rahmlow, "New Performance Levels for TPV Front Surface Filters," in *AIP Conference Proceedings*, Freiburg (Germany): AIP, 2004, pp. 180–188. doi: 10.1063/1.1841893.
- [79] O. Vigil, C. M. Ruiz, D. Seuret, V. Bermúdez, and E. Diéguez, "Transparent conducting oxides as selective filters in thermophotovoltaic devices," *J. Phys. Condens. Matter*, vol. 17, no. 41, pp. 6377–6384, Oct. 2005, doi: 10.1088/0953-8984/17/41/008.
- [80] Joannopoulos, J. D., Johnson, S. G., Winn, J. N., & Meade, R. D, *Photonic crystals: Molding the flow of light. In Photonic Crystals: Molding the Flow of Light (Second Edition)*. Princeton University Press, 2008.
- [81] A. Pirvaram, N. Talebzadeh, M. Rostami, S. N. Leung, and P. G. O'Brien, "Evaluation of a ZrO<sub>2</sub>/ZrO<sub>2</sub>-aerogel one-dimensional photonic crystal as an optical filter for thermophotovoltaic applications," *Therm. Sci. Eng. Prog.*, vol. 25, p. 100968, Oct. 2021, doi: 10.1016/j.tsep.2021.100968.
- [82] W. Belhadj, A. Timoumi, H. Dakhlaoui, and F. Alhashmi Alamer, "Design and Optimization of One-Dimensional TiO<sub>2</sub>/GO Photonic Crystal Structures for Enhanced Thermophotovoltaics," *Coatings*, vol. 12, no. 2, p. 129, Jan. 2022, doi: 10.3390/coatings12020129.
- [83] F. O'Sullivan, I. Celanovic, N. Jovanovic, J. Kassakian, S. Akiyama, and K. Wada, "Optical characteristics of one-dimensional Si/SiO<sub>2</sub> photonic crystals for thermophotovoltaic applications," *J. Appl. Phys.*, vol. 97, no. 3, p. 033529, Feb. 2005, doi: 10.1063/1.1849437.
- [84] G. Liu, Y. Xuan, Y. Han, and Q. Li, "Investigation of one-dimensional Si/SiO<sub>2</sub> photonic crystals for thermophotovoltaic filter," *Sci. China Ser. E Technol. Sci.*, vol. 51, no. 11, pp. 2031–2039, Nov. 2008, doi: 10.1007/s11431-008-0139-0.
- [85] L. Mao and H. Ye, "New development of one-dimensional Si/SiO<sub>2</sub> photonic crystals filter for thermophotovoltaic applications," *Renew. Energy*, vol. 35, no. 1, pp. 249–256, Jan. 2010, doi: 10.1016/j.renene.2009.06.013.
- [86] Fabrice Kwefeu Mbakop, "Transmission of light through an optical filter of a one-dimensional photonic crystal: application to the solar thermophotovoltaic system," 2017.
- [87] S. I. Mostafa, N. H. Rafat, and S. A. El-Naggar, "One-dimensional metallic-dielectric (Ag/SiO<sub>2</sub>) photonic crystals filter for thermophotovoltaic applications," *Renew. Energy*, vol. 45, pp. 245–250, Sep. 2012, doi: 10.1016/j.renene.2012.03.001.
- [88] S. G. Babiker, Y. Shuai, M. O. Sid-Ahmed, and M. Xie, "One –Dimensional Si/SiO<sub>2</sub> Photonic Crystals Filter for Thermophotovoltaic Applications," vol. 9, 2014.
- [89] F. K. Mbakop, N. Djongyang, and D. Raïdandi, "One–dimensional TiO<sub>2</sub>/SiO<sub>2</sub> photonic crystal filter for thermophotovoltaic applications," *J. Eur. Opt. Soc.-Rapid Publ.*, vol. 12, no. 1, p. 23, Dec. 2016, doi: 10.1186/s41476-016-0026-4.
- [90] F. K. Mbakop, A. Tom, A. Dadjé, A. K. C. Vidal, and N. Djongyang, "One-dimensional comparison of TiO<sub>2</sub>/SiO<sub>2</sub> and Si/SiO<sub>2</sub> photonic crystals filters for thermophotovoltaic applications in visible and infrared," *Chin. J. Phys.*, vol. 67, pp. 124–134, Oct. 2020, doi: 10.1016/j.cjph.2020.06.004.
- [91] F. K. Khosroshahi, H. Ertürk, and M. Pınar Mengüç, "Optimization of spectrally selective Si/SiO<sub>2</sub> based filters for thermophotovoltaic devices," *J. Quant. Spectrosc. Radiat. Transf.*, vol. 197, pp. 123–131, Aug. 2017, doi: 10.1016/j.jqsrt.2017.01.030.

- [92] K. Binidra, R. Miloua, M. Khadraoui, Z. Kebbab, A. Bouzidi, and N. Benramdane, "Spectral control in thermophotovoltaic systems by optimized one-dimensional photonic crystals," *Optik*, vol. 156, pp. 879–885, Mar. 2018, doi: 10.1016/j.ijleo.2017.12.070.
- [93] S. Shi, A. Sharkawy, C. Chen, D. M. Pustai, and D. W. Prather, "Dispersion-based beam splitter in photonic crystals," *Opt. Lett.*, vol. 29, no. 6, p. 617, Mar. 2004, doi: 10.1364/OL.29.000617.
- [94] S. Guldin *et al.*, "Dye-Sensitized Solar Cell Based on a Three-Dimensional Photonic Crystal," *Nano Lett.*, vol. 10, no. 7, pp. 2303–2309, Jul. 2010, doi: 10.1021/nl904017t.
- [95] S. Shoji and S. Kawata, "Photofabrication of three-dimensional photonic crystals by multibeam laser interference into a photopolymerizable resin," *Appl. Phys. Lett.*, vol. 76, no. 19, pp. 2668–2670, May 2000, doi: 10.1063/1.126438.
- [96] F. Iskandar, "Nanoparticle processing for optical applications – A review," *Adv. Powder Technol.*, vol. 20, no. 4, pp. 283–292, Jul. 2009, doi: 10.1016/j.apt.2009.07.001.
- [97] Schmid, Günter, ed, *Nanoparticles: from theory to application*. John Wiley & Sons, 2011.
- [98] S. M. Weiss, M. Haurylau, and P. M. Fauchet, "Tunable photonic bandgap structures for optical interconnects," *Opt. Mater.*, vol. 27, no. 5, pp. 740–744, Feb. 2005, doi: 10.1016/j.optmat.2004.08.007.
- [99] A. Mehaney, M. M. Abadla, and H. A. Elsayed, "1D porous silicon photonic crystals comprising Tamm/Fano resonance as high performing optical sensors," *J. Mol. Liq.*, vol. 322, p. 114978, Jan. 2021, doi: 10.1016/j.molliq.2020.114978.
- [100] F. Chi, L. Yan, H. Lv, C. Wang, and X. Yuan, "Effect of polyvinyl butyral on the microstructure and laser damage threshold of antireflective silica films," *Thin Solid Films*, vol. 519, no. 8, pp. 2483–2487, Feb. 2011, doi: 10.1016/j.tsf.2010.11.023.
- [101] F. Iskandar, Mikrajuddin, and K. Okuyama, "In Situ Production of Spherical Silica Particles Containing Self-Organized Mesopores," *Nano Lett.*, vol. 1, no. 5, pp. 231–234, May 2001, doi: 10.1021/nl0155227.
- [102] F. Iskandar, M. Abdullah, H. Yoden, and K. Okuyama, "Optical band gap and ultralow dielectric constant materials prepared by a simple dip coating process," *J. Appl. Phys.*, vol. 93, no. 11, pp. 9237–9242, Jun. 2003, doi: 10.1063/1.1571218.
- [103] F. Iskandar, M. Abdullah, H. Yoden, and K. Okuyama, "Silica Films Containing Ordered Pores Prepared by Dip Coating of Silica Nanoparticles and Polystyrene Beads Colloidal Mixture," *J. Sol-Gel Sci. Technol.*, vol. 29, no. 1, pp. 41–47, Jan. 2004, doi: 10.1023/B:JSST.0000016136.39875.24.
- [104] M. E. Calvo, O. Sánchez-Sobrado, S. Colodrero, and H. Míguez, "Control over the Structural and Optical Features of Nanoparticle-Based One-Dimensional Photonic Crystals," *Langmuir*, vol. 25, no. 4, pp. 2443–2448, Feb. 2009, doi: 10.1021/la8030057.
- [105] J. H. Prosser, T. Brugarolas, S. Lee, A. J. Nolte, and D. Lee, "Avoiding Cracks in Nanoparticle Films," *Nano Lett.*, vol. 12, no. 10, pp. 5287–5291, Oct. 2012, doi: 10.1021/nl302555k.
- [106] J.-Q. Xi *et al.*, "Optical thin-film materials with low refractive index for broadband elimination of Fresnel reflection," *Nat. Photonics*, vol. 1, no. 3, pp. 176–179, Mar. 2007, doi: 10.1038/nphoton.2007.26.
- [107] U. Schulz, F. Rickelt, H. Ludwig, P. Munzert, and N. Kaiser, "Gradient index antireflection coatings on glass containing plasma-etched organic layers," *Opt. Mater. Express*, vol. 5, no. 6, p. 1259, Jun. 2015, doi: 10.1364/OME.5.001259.
- [108] X. Wang, H. Masumoto, Y. Someno, and T. Hirai, "Design and experimental approach of optical reflection filters with graded refractive index profiles," *J. Vac. Sci. Technol. Vac. Surf. Films*, vol. 17, no. 1, pp. 206–211, Jan. 1999, doi: 10.1116/1.581574.
- [109] G. Wu *et al.*, "Preparation and properties of scratch-resistant nanoporous broadband AR silica films derived by a two-step catalytic sol-gel process," presented at the 4th International Conference on Thin Film Physics and Applications, J. Chu, P. Liu, and Y. Chang, Eds., Shanghai, China, Nov. 2000, p. 807. doi: 10.1117/12.408386.

- [110] D. P. Partlow and T. W. O’Keeffe, “Thirty-seven layer optical filter from polymerized solgel solutions,” *Appl. Opt.*, vol. 29, no. 10, p. 1526, Apr. 1990, doi: 10.1364/AO.29.001526.
- [111] G. Wicht, R. Ferrini, S. Schüttel, and L. Zuppiroli, “Nanoporous Films with Low Refractive Index for Large-Surface Broad-Band Anti-Reflection Coatings,” *Macromol. Mater. Eng.*, vol. 295, no. 7, pp. 628–636, Jul. 2010, doi: 10.1002/mame.201000045.
- [112] A. Hojabri, “Structural and optical characterization of ZrO<sub>2</sub> thin films grown on silicon and quartz substrates,” *J. Theor. Appl. Phys.*, vol. 10, no. 3, pp. 219–224, Sep. 2016, doi: 10.1007/s40094-016-0218-8.
- [113] J. K. Kim *et al.*, “Light-Extraction Enhancement of GaInN Light-Emitting Diodes by Graded-Refractive-Index Indium Tin Oxide Anti-Reflection Contact,” *Adv. Mater.*, vol. 20, no. 4, pp. 801–804, Feb. 2008, doi: 10.1002/adma.200701015.
- [114] Y.-H. Hsiao *et al.*, “Light extraction enhancement with radiation pattern shaping of LEDs by waveguiding nanorods with impedance-matching tips,” *Nanoscale*, vol. 6, no. 5, pp. 2624–2628, 2014, doi: 10.1039/C3NR05226E.
- [115] M.-L. Kuo *et al.*, “Realization of a near-perfect antireflection coating for silicon solar energy utilization,” *Opt. Lett.*, vol. 33, no. 21, p. 2527, Nov. 2008, doi: 10.1364/OL.33.002527.
- [116] Y. Jiang *et al.*, “Optical and interfacial layer properties of SiO<sub>2</sub> films deposited on different substrates,” *Appl. Opt.*, vol. 53, no. 4, p. A83, Feb. 2014, doi: 10.1364/AO.53.000A83.
- [117] R. Yusoh, M. Horprathum, P. Eiamchai, P. Chindaudom, and K. Aiempanakit, “Determination of Optical and Physical Properties of ZrO<sub>2</sub> Films by Spectroscopic Ellipsometry,” *Procedia Eng.*, vol. 32, pp. 745–751, 2012, doi: 10.1016/j.proeng.2012.02.007.
- [118] Q. Zhang, J. Shen, J. Wang, G. Wu, and L. Chen, “Sol-gel derived ZrO<sub>2</sub>-SiO<sub>2</sub> highly reflective coatings,” *Int. J. Inorg. Mater.*, vol. 2, no. 4, pp. 319–323, Sep. 2000, doi: 10.1016/S1466-6049(00)00037-4.
- [119] D. A. Weitz, “Packing in the Spheres,” *Science*, vol. 303, no. 5660, pp. 968–969, Feb. 2004, doi: 10.1126/science.1094581.
- [120] W. M. Yang, S. K. Chou, C. Shu, Z. W. Li, and H. Xue, “Experimental study of micro-thermophotovoltaic systems with different combustor configurations,” *Energy Convers. Manag.*, vol. 48, no. 4, pp. 1238–1244, Apr. 2007, doi: 10.1016/j.enconman.2006.10.002.
- [121] Y. Xuan, X. Chen, and Y. Han, “Design and analysis of solar thermophotovoltaic systems,” *Renew. Energy*, vol. 36, no. 1, pp. 374–387, Jan. 2011, doi: 10.1016/j.renene.2010.06.050.
- [122] S.-H. Lee, A. R. B. M. Yusoff, C. Lee, S. C. Yoon, and Y.-Y. Noh, “Toward color-selective printed organic photodetectors for high-resolution image sensors: From fundamentals to potential commercialization,” *Mater. Sci. Eng. R Rep.*, vol. 147, p. 100660, Jan. 2022, doi: 10.1016/j.mser.2021.100660.
- [123] Jin, Jian-Ming. *The finite element method in electromagnetics*. John Wiley & Sons, 2015.
- [124] P. Yeh, *Optical Waves in Layered Media* (Wiley, New York, 1988), pp. 118 – 123.
- [125] C. Houck, J. Joines, and M. Kay, “A Genetic Algorithm for Function Optimization: a Matlab Implementation,” *Tech. Rep. NCSU-IE Tr 95-09* (North Carolina State University, Raleigh, N.C., 1995).
- [126] B. J. Hoenders and M. Bertolotti, “Coherence theory of electromagnetic wave propagation through stratified N-layer media,” *J. Opt. Soc. Am. A*, vol. 22, no. 6, p. 1143, Jun. 2005, doi: 10.1364/JOSAA.22.001143.
- [127] P. Berning, *Phys. Thin Films*, 1 (1963) 69 - 121.
- [128] F. Ab-les, in A. C. S. Van Hell (ed.), *Advanced Optical Techniques*, North-Holland, Amsterdam, 1967, p. 178.
- [129] P. M. Martin, L. C. Olsen, J. W. Johnston, and D. M. DePoy, “Sputtered Si:H alloys for edge filters: application to thermophotovoltaics,” *Appl. Opt.*, vol. 41, no. 31, p. 6702, Nov. 2002, doi: 10.1364/AO.41.006702.

- [130] P. M. Martin, L. C. Olsen, J. W. Johnston, and D. M. Depoy, "Investigation of sputtered HfF<sub>4</sub> films and application to interference filters for thermophotovoltaics," *Thin Solid Films*, vol. 420–421, pp. 8–12, Dec. 2002, doi: 10.1016/S0040-6090(02)00652-1.
- [131] H. Yu, Z. Ikonic, D. Indjin, and R. W. Kelsall, "The effect of interface roughness on spectral efficiency of thermophotovoltaics with multi-layer filters," *Optik*, vol. 257, p. 168663, May 2022, doi: 10.1016/j.ijleo.2022.168663.
- [132] S. Miyazaki, Y. Hamamoto, E. Yoshida, M. Ikeda, and M. Hirose, "Control of self-assembling formation of nanometer silicon dots by low pressure chemical vapor deposition," *Thin Solid Films*, vol. 369, no. 1–2, pp. 55–59, Jul. 2000, doi: 10.1016/S0040-6090(00)00834-8.
- [133] S. Peng and G. M. Morris, "Efficient implementation of rigorous coupled-wave analysis for surface-relief gratings," *J. Opt. Soc. Am. A*, vol. 12, no. 5, p. 1087, May 1995, doi: 10.1364/JOSAA.12.001087.
- [134] D. R. Huanca, "Optical and Structural Characterization of One-Dimensional Porous Silicon Photonic Crystals Made Using Single and Double Thank Electrochemical Cell." Rochester, NY, Feb. 10, 2023. doi: 10.2139/ssrn.4354245.